International Journal of Remote Sensing

ISSN: 0143-1161 (Print) 1366-5901 (Online) Journal homepage: http://www.tandfonline.com/loi/tres20

SAR polarimetry for sea oil slick observation

M. Migliaccio, F. Nunziata & A. Buono

To cite this article: M. Migliaccio, F. Nunziata & A. Buono (2015) SAR polarimetry for sea oil slick observation, International Journal of Remote Sensing, 36:12, 3243-3273, DOI: 10.1080/01431161.2015.1057301

To link to this article: http://dx.doi.org/10.1080/01431161.2015.1057301

International Journal of Remote Sensing, 2015
Vol. 36, No. 12, 3243–3273, http://dx.doi.org/10.1080/01431161.2015.1057301

Taylor & Francis
Taylor & Francis Group

REVIEW ARTICLE

SAR polarimetry for sea oil slick observation

M. Migliaccio*, F. Nunziata, and A. Buono

Dipartimento di Ingegneria, Centro Direzionale isola C4, Università degli Studi di Napoli Parthenope, Napoli, Italy

(*Received 11 March 2015; accepted 26 May 2015*)

In this article, a review of polarimetric synthetic aperture radar (SAR) methods for sea oil slick observation is presented. Marine oil pollution monitoring is a topic of great applicative and scientific relevance. In this framework, the use of remotely sensed measurements is of special interest and, in particular, the SAR because of its almost all-weather and all-day imaging capability at fine spatial resolution is the most effective tool. Conventional single-polarization SAR oil spill monitoring techniques are limited in their capability to detect oil slicks since they strongly rely on suitable thresholds, training samples, and ancillary information. Hence, an expert image analyst is due. The launch of a number of polarimetric SAR missions, along with the understanding of the peculiar physical mechanisms governing the scattering by an oil slick, led to a new paradigm (known as physical processing) that fostered a set of polarimetric algorithms particularly robust and efficient. Hence, suitable polarimetric models that exploit the departure from the slick-free sea Bragg scattering have been developed to effectively address oil slick monitoring. A set of polarimetric features extracted following such electromagnetic models have been proved to be reliable for oil slick monitoring. Polarimetric SAR observations led to a significant improvement in sea oil slick observation since they allow distinguishing oil slicks from a broad class of lookalikes in an unsupervised way. In addition, deeper information on the damping properties of the pollutant can be also inferred, which is of paramount importance for remediation purposes. Such physical processing has been demonstrated to be robust at variance of microwave carrier frequency, e.g. L-, C-, and X-band, and suitable to be exploited to extract information by dual-polarized, full-polarized, and compact modes. All these make such a physical approach of operational interest since it is able to exploit a larger set of SAR measurements building up a virtual constellation. In this review all these are detailed.

1. Introduction

It is worldwide recognized that a large amount of oil is yearly discharged into the marine environment due to vessel operations, land-based sources, etc. and that coastal environments suffer from petroleum pollutants. The topic is very relevant and it includes the different sources of sea oil spills, how they are affected by weathering and other physical processes, i.e. evaporation, dispersion, emulsification, and what are the effects of oil discharged into the sea on marine ecosystems. In 2003, it was estimated that every year more than 380 million gallons of oil are released into the sea, although the ecological impact of such oil spills is related to the geographical location more than the size (NRC 2003).

*Corresponding author. Email: maurizio.migliaccio@uniparthenope.it

Oil sources can be classified into four categories: natural oil seeps, petroleum extraction, petroleum transportation, and petroleum consumption (NRC 2003). Oil seeps are natural hydrocarbon stocks characterized by natural low-rate escape of liquid or gaseous crude oil and tar, also known as oil seepages, to the Earth's atmosphere and surface due to low pressure conditions or flow (WHOI 2011). It was estimated that about 45% of crude oil entering into the marine environment comes from oil seepages, for an amount of about 180 million gallons per year (NRC 2003).

Petroleum extraction is represented by all the crude oil and refined products associated with human activities undertaken for petroleum production and exploration purposes. The characteristics of such oil spills are highly variable in terms of the nature and size, but they are strictly related to active oil and gas exploration and development areas. In ocean areas rich in oil seeps, e.g. off the coasts of California and in the Gulf of Mexico, there are several oil and gas platforms that strongly contribute to oil released into the sea. Annually, about 11 million gallons of oil products linked to extraction and exploration activities are discharged. They represent about 5% of the total oil entering into the marine environment (NRC 2003). Nonetheless, recently, although there has been a significant decrease in the amount of petroleum released during extraction activities, when dealing with old infrastructures, the threat of potential oil spill is relevant.

Petroleum transportation includes both small-size operational oil spills that regularly occur and large oil spills due to accidental disasters such as the Exxon Valdez and Prestige tankers ones. Crude oil and refined products due to distribution and refining activities are spilled into the sea for an overall amount of about 44 million gallons (less than 22%) (NRC 2003). This kind of oil spill can occur everywhere, especially along main tankers' routes or where pipelines are mostly located. Therefore, oil spills due to transportation activities are characterized by a broad range of oils in terms of their physical and chemical properties.

Petroleum consumption consists of all the oil products associated with activities which need petroleum to be performed. Hence, they are typically small but widespread frequent releases that represent a random but consistent amount of oil entering into the ocean environment due to human activities (about 140 million gallons every year) (NRC 2003). Oil discharging due to petroleum consumption contributes to about 70% of the total amount of oil released into the sea due to sources related to human activities. This kind of source is characterized by slow and chronic release of oil into the ocean environment through rivers and wastewater streams. Within such a context, a unique case is represented by the Transocean Deepwater Horizon oil accident occurred in the Gulf of Mexico on 20 April 2010, in which the burning and sinking of a British Petroleum oil rig led to an uncontrolled discharge of an estimated amount of little less than 4 million of petroleum barrels (corresponding to about 210 million gallons) from the 1500 m deep Macondo well (NOAA 2012). This huge oil spill covered tens of thousands square kilometres and it involved a continuous releasing source at a depth of 1.5 km. Therefore, massive use of chemical dispersants was made to minimize its environmental impact and the spilled oil was subjected to various weathering processes. In such a case, the main issue is not detecting the oil spill, but to understand the physical behaviour of the spilled oil and to investigate its space-time evolution. Although different studies have been undertaken witnessing the key role played by remote-sensing tools, with particular reference to airborne and spaceborne polarimetric SARs, this still remains a very critical and challenging case (Migliaccio et al. 2011; Jones et al. 2011; Migliaccio, Nunziata, Brown, et al. 2012; Migliaccio and Nunziata 2014; Collins et al. 2015). The results have shown that the aforementioned peculiar oil spill characteristics led to a complex oil characterization

mostly due to weathering phenomena, dispersants usage, and oil-in-water mixing which hampered natural mineral oil properties resulting in a totally different scattering behaviour. Furthermore, recent studies have shown that nowadays, it is reasonable to affirm that about 3200 square kilometres of the ocean region close to the Macondo well is contaminated by a fallout plume of submerged oil and that this represents only less than 35% of the sequestered oil deposited on the ocean floor outside that area (Valentine et al. 2014).

Sea oil slick observation represents a key topic where end user needs, technological advance and physical modelling that are perfectly mixed. The main needs arise from the end user community (e.g. operational surveillance and monitoring agencies, stakeholders in oil and gas sectors that are interested in both oil spill response and reservoir search activity) are:

- sea oil slick detection, i.e. discriminating oil from both the surrounding sea and natural features that look like oil, termed oil lookalikes;
- characterizing the detected oil slick, i.e. providing at least rough information on the physical–chemical properties of the spilled oil.

From a technological perspective, the most effective tool to ensure a synoptic and detailed oil spill monitoring is imaging remote sensing. Within this context, the all-day and almost all-weather measurements offered by the synthetic aperture radar (SAR), a microwave fine spatial resolution imaging radar, make it the key remote-sensing instrument for operational sea oil slick observation (Solberg 2012). However, SAR-based sea oil slick monitoring is not an easy task. From a physical viewpoint, an oil slick dampens the short gravity and capillary Bragg scattering ocean waves resulting in a low backscatter area. The latter appears in conventional single-polarization SAR intensity grey-tone imagery as a dark patch (Fingas and Brown 1997; Nunziata, Sobieski, and Migliaccio 2009). However, there are many natural phenomena (e.g. low-wind areas, oceanic currents, grease ice, biogenic surfactants, etc.) which, resulting in a similar reduction of Bragg scattering ocean waves, produce dark patches in single-polarization intensity SAR images that are almost indistinguishable from the oil ones (Fingas and Brown 1997; Nunziata, Sobieski, and Migliaccio 2009). Particularly critical is the oil slick observation over the Arctic region, where both oil and thin sea ice have similar low backscattering in single-polarization SAR imagery, making the operational monitoring a challenging task (Brekke et al. 2014). Accordingly, to perform oil/lookalike discrimination in single-polarization SAR imagery a computer-time expensive three-step procedure is generally implemented that basically consists of (Fingas and Brown 1997; Solberg et al. 1999; Brekke and Solberg 2005; Migliaccio, Gambardella, and Tranfaglia 2007; Solberg, Brekke, and Husoy 2007; Brekke and Solberg 2008; Gambardella et al. 2010; Fingas and Brown 2015): dark area detection, feature extraction, and oil/lookalike discrimination. Single-polarization methods are limited in their ability to observe sea oil slicks due to their dependence on thresholding techniques, training samples, and ancillary external information (Fingas and Brown 1997; Gambardella et al. 2010; Solberg 2012; Fingas and Brown 2015). In addition, since oil discrimination, i.e. identification of oil slicks among the detected dark areas, is performed on the basis of extracted features related to oil morphological complexity; when dealing with huge mineral oil spills, diffuse low-wind fields or wide algal blooms, the SAR image can consist of a whole dark patch, thus making such techniques practically unusable. Hence, a trained expert image analyst is often needed to eventually

sort out actual oil spill from the detected dark areas, and no information on the physical and chemical properties of the spilled oil, that could be useful for remediation purposes, can be inferred.

The technological development of the space industry led to the launch of several high-performance SAR satellites that are equipped with polarimetric modes: the L-band Japanese Aerospace Exploration Agency (JAXA), Advanced Land Observing Satellite (ALOS), (Phased Array type L-band SAR (PALSAR), and its follow on ALOS PALSAR-2, the C-band Canadian Space Agency (CSA) Radarsat-2 and its follow on Radarsat Constellation Mission (RCM), together with the C-band Indian Space Research Organisation (ISRO) Risat-1 (Radar Imaging Satellite), and the X-band German Aerospace Center (DLR) TerraSAR-X and Italian Space Agency (ASI) Constellation of small Satellites for the Mediterranean basin Observation (Cosmo-SkyMed) (see Table 1). In Table 1, the progress of polarimetric spaceborne SAR architectures is summarized, from the first fully polarimetric SAR sensor, Spaceborne Imaging Radar (SIR) C/X, launched by National Aeronautics and Space Administration (NASA) in 1994 and by now dismissed, to the near future polarimetric satellite missions equipped with CP SAR configurations already planned for next years as RCM and the National Space Activities Commission (CONAE) Spanish for Argentine Microwaves Observation Satellite (SAOCOM), passing through the actually operational Risat-1 and ALOS PALSAR-2. In the literature, spaceborne fully/dual-polarized L-, C-, and X-band SAR data have been exploited for sea oil slick monitoring (Migliaccio, Nunziata, and Gambardella 2009; Migliaccio, Nunziata, Montuori, et al. 2012; Zhang et al. 2011; Velotto et al. 2011; Kudryavtsev et al. 2013; Matkan, Hajeb, and Azarakhsh 2014; Skrunes, Brekke, and Eltoft 2014; Skrunes et al. 2014). Different polarimetric techniques have been successfully applied to detect ship-based oil spills, to monitor and support remediation activities in the case of large accidental oil spills, and to observe natural oil seeps. In addition, the challenging investigation of oil in sea ice scenarios can be performed exploiting polarimetric approaches (Brekke et al. 2014).

Furthermore, some airborne polarimetric SARs have been also designed and operated for oil spill services, as the L-band NASA Jet Propulsion Laboratory (JPL) Uninhabited Aerial Vehicle Synthetic Aperture Radar (UAVSAR) (Jones et al. 2011; Minchew, Jones, and Holt 2012; Minchew 2012; Migliaccio and Nunziata 2014). The latter, still operating since 2007, provides high quality fully polarimetric SAR data with very low noise floor (less than −35 dB), fine spatial resolution (3 m × 1 m) offering a 22 km swath width. Before proceeding further, it must be noted that enabling technologies for spaceborne and airborne polarimetric SAR are not all identical. Furthermore, the sensor specifications and tests to be passed are very different. Generally speaking, the airborne SARs show better performance but suffer from several drawbacks such as motion compensation, lifetime mission, and data coverage. In real life, it is advisable to combine satellite-based SAR measurements with airborne ones to guarantee an effective oil service. Of course, it is important that relevant polarimetric SAR features are well-estimated, i.e. the underlying polarimetric measurements are reliable, and polarimetric SAR data are characterized by satisfactory quality (Touzi et al. 1993; Touzi, Vachon, and Wolfe 2010; Skrunes et al. 2014). Note that one of the limiting factors is the noise floor, especially when dealing with the cross-polarized channel. Since the cross-polarized channel is characterized by the weakest return, its signal level could be below the noise floor, thus affecting characterization performance. Of course, this does not represent an issue when dealing with oil detection.

Table 1. Spaceborne polarimetric SAR missions.

Mission/SAR	Agency	Period	Status	Mode	Frequency (BAND)	NESZ (dB)	Spatial resolution (slant rg. × az.) (m)	Coverage (rg. × az.) (km)
SIR C/X	NASA	1994–2005	Decomissioned	Fully polarimetric	L, C	–28 (C)	20.12 × 8.16	15–90 × 15–90
ENVISAT ASAR	ESA	2002–2012	Decomissioned	Dual-polarimetric (incoherent)	C	≤– 20	30 × 30	100 × 100
ALOS PALSAR	JAXA	2006–2011	Decomissioned	Fully polarimetric	L	–30	9.4 × 4.5	30 × 30
RADARSAT 2	CSA	2007–present	Operational	Fully polarimetric	C	–36.5 ± 3	5.2 × 7.6	25 × 25
COSMO-SKYMED	ASI	2007–present	Operational	Dual-polarimetric (incoherent)	X	≤–22	15 × 15	30 × 30
TERRASAR-X	DLR	2007–present	Operational	Dual-/fully polarimetric	X	–19 to –26	3 × 2.2	10 × 10
RISAT 1	ISRO	2012–present	Operational	Dual-/compact-/fully polarimetric	C	≤–19	6 × 4	25 × 25
ALOS PALSAR 2	JAXA	2014–present	Operational	Dual-/compact-/fully polarimetric	L	–28	10 × 10	30 × 30
SENTINEL 1	ESA	2014–present	Operational	Dual-polarimetric	C	≤– 22	2.7 × 22	250 × 250
SAOCOM	CONAE/ASI	2018–2023	Planned	Dual-/compact-/fully polarimetric	L	–	<10 × 10	15–44 × 15–44
RCM	CSA	2018–2025	In development	Compact-/fully polarimetric	C	≤–22	15 × 9	25 × 25
COSMO-SKYMED 2	ASI	2019–2027	Approved	Dual-/fully polarimetric	X	–	3 × 3	15 × 250
BIOMASS	ESA	2020–2025	Planned	Compact-/fully polarimetric	P	≤–27	≤50 × 50	≥100 × 100

Note: The characteristics listed refer to the finest spatial resolution polarimetric mode.

As a matter of fact, the wide distribution of polarimetric data sets across the remote-sensing community boosted activities and developments in polarimetric SAR applications. However, although there was a general consensus that radar polarimetry is able to provide additional information to environmental applications, the real benefit of polarimetric information was demonstrated only for land applications and first investigations on sea oil slick observation were generally unsatisfactory (Gade et al. 1998). The key role played by SAR polarimetry in sea oil slick monitoring was first shown by Migliaccio, Gambardella, and Tranfaglia (2007); Migliaccio, Nunziata, and Gambardella (2009), where polarimetric information was demonstrated to be of paramount importance to both detect sea oil slicks and distinguish them from a broad range of lookalikes, i.e. those characterized by weak-damping properties. Since then, polarimetric models and analysis tools have been developed and applied to actual polarimetric L-, C-, and X-band SAR data. All the polarimetric approaches share a common physical rationale, which is the Bragg scattering model that well-describes both slick-free and weak-damping slick-covered sea surface scattering under low-to-moderate wind conditions and at intermediate angles of incidence. A completely different scattering behaviour applies when dealing with strong-damping oil-covered sea surface, i.e. a non-Bragg scattering mechanism applies (Migliaccio, Gambardella, and Tranfaglia 2007; Nunziata, Gambardella, and Migliaccio 2008; Migliaccio, Nunziata, and Gambardella 2009; Nunziata, Migliaccio, and Gambardella 2011). Hence, following this theoretical rationale, a set of polarimetric features is defined and used to measure the departure from Bragg scattering. Nonetheless, on a technical side, fully polarimetric SAR modes are characterized by a very limited swath width and spatial resolution (see Table 1), which hamper their operational use. Recently, the technological development led to new SAR architectures, e.g. the staggered SAR (Villano, Krieger, and Moreira 2014) and compact-polarimetry (CP) modes (Raney 2007, 2011). The former guarantees a fine spatial resolution continuous imaging of a wide swath combining digital beamforming and a variable pulse repetition interval. The underpinning idea of CP SAR architectures consists of implementing a coherent dual-polarimetric system where, instead of transmitting a conventional linear polarization (horizontal, h, or vertical, v) different configurations are considered, i.e. slant linear ($\pi/4$) or circular, while receiving coherently in an orthogonal basis (Raney 2007, 2011; Sabry and Vachon 2014). This ensures a swath width significantly larger than the one provided by a fully polarimetric SAR system, with polarimetric performance that tends to the fully polarimetric one. This technological progress boosted the development of new techniques to exploit CP SAR for sea oil slick monitoring purposes (Shirvany, Chabert, and Tourneret 2012; Nunziata, Migliaccio, and Li 2015; Salberg, Rudjord, and Solberg 2014; Paes, Nunziata, and Migliaccio, forthcoming; Nunziata and Migliaccio 2014; Yin et al., forthcoming; Li et al. 2015).

In this review, the main outcomes relevant to polarimetric SAR for sea oil slick observation are critically reviewed in terms of the operational results that the different polarimetric SAR architectures allow obtaining. First, the polarimetric backbone that allows comprehending the different polarimetric SAR approaches is reviewed, and then some key experiments are undertaken on actual L- and C-band SAR data to critically discuss capabilities and performance of the different approaches.

2. SAR polarimetry background

In this section, the polarimetric background that lies at the basis of the approaches developed to observe sea oil slicks is reviewed. Basic wave polarization concepts that

allow an easy physical understanding of the methods recently developed to exploit CP SAR architectures are also described.

2.1. Polarimetric scattering descriptors

The theoretical polarimetric background required to understand polarimetric SAR measurements and to correctly extract and interpret polarimetric information is here presented.

A fully polarimetric SAR measures the scattering matrix **S** that rules the transformation of the incident electric field into the one scattered off the observed scene. According to the Jones formalism, the relationship between the incident and the scattered wave is given by (Guissard 1994):

$$\boldsymbol{E}^{\mathrm{s}} = \frac{e^{-jkr}}{r}\mathbf{S}\boldsymbol{E}^{\mathrm{i}}, \tag{1}$$

where j is the imaginary unit, k is the electromagnetic wavenumber, r is the distance between the SAR antenna and the centre of the imaged scene, and $\boldsymbol{E}^{\mathrm{s}}$ and $\boldsymbol{E}^{\mathrm{i}}$ are the complex Jones vectors describing the scattered and incident field, respectively. **S** is a 2×2 complex matrix that, when the linear $\{h, v\}$ basis is adopted and when reciprocity holds, is given by

$$\mathbf{S} = \begin{pmatrix} S_{\mathrm{hh}} & S_{\mathrm{hv}} \\ S_{\mathrm{hv}} & S_{\mathrm{vv}} \end{pmatrix}, \tag{2}$$

whose complex elements S_{pq}, with $p,\ q \in \{h, v\}$, are known as scattering amplitudes. It is important to underline that, for a given frequency and viewing geometry, the scattering matrix depends only on the scattering properties of the observed scene (Cloude 2009). Equation (2) represents a first-order coherent scattering model which, relying on the Jones formalism, does not allow describing depolarizing phenomena.

The most powerful way to deal with polarimetric scattering from a distributed and depolarizing scene is to use the second-order products of the scattering matrix (Van Zyl, Papas, and Elachi 1987). Either an incoherent model, based on the Stokes formalism, or a coherent approach, based on the coherence **T** or covariance **C** matrices, can be used (Cloude and Pottier 1996). According to the Stokes formalism, the scattered field (described by the Stokes vector $\boldsymbol{s}^{\mathrm{s}}$) is related to the incident field $\boldsymbol{s}^{\mathrm{i}}$ by the 4×4 matrix **M**, that is termed Mueller matrix:

$$\boldsymbol{s}^{\mathrm{s}} = (kr)^{-2}\mathbf{M}\boldsymbol{s}^{\mathrm{i}}. \tag{3}$$

M is a real and never symmetric matrix whose elements are ensemble averages of combinations of the scattering amplitudes (Guissard 1994). In the backscattering case, assuming a back scattering alignment (BSA) convention and the reciprocity, the elements of **M** are given by (Guissard 1994)

$$
\begin{aligned}
M_{11} &= \frac{1}{2}\langle |S_{\mathrm{hh}}|^2 + 2|S_{\mathrm{hv}}|^2 + |S_{\mathrm{vv}}|^2 \rangle, \\
M_{22} &= \frac{1}{2}\langle |S_{\mathrm{hh}}|^2 - 2|S_{\mathrm{hv}}|^2 + |S_{\mathrm{vv}}|^2 \rangle, \\
M_{33} &= \langle \Re(S_{\mathrm{hh}} S_{\mathrm{vv}}{}^* + |S_{\mathrm{hv}}|^2) \rangle, \\
M_{44} &= \langle \Re(S_{\mathrm{hh}} S_{\mathrm{vv}}{}^* - |S_{\mathrm{hv}}|^2) \rangle, \\
M_{12} &= M_{21} = \frac{1}{2}\langle (|S_{\mathrm{hh}}|^2 - |S_{\mathrm{vv}}|^2) \rangle, \\
M_{13} &= M_{31} = \langle \Re(S_{\mathrm{hh}} S_{\mathrm{hv}}{}^* + S_{\mathrm{hv}} S_{\mathrm{vv}}{}^*) \rangle, \\
M_{14} &= -M_{41} = \langle \Im(S_{\mathrm{hh}} S_{\mathrm{hv}}{}^* + S_{\mathrm{hv}} S_{\mathrm{vv}}{}^*) \rangle, \\
M_{23} &= M_{32} = \langle \Im(S_{\mathrm{hh}} S_{\mathrm{hv}}{}^* - S_{\mathrm{hv}} S_{\mathrm{vv}}{}^*) \rangle, \\
M_{24} &= -M_{42} = \langle \Im(S_{\mathrm{hh}} S_{\mathrm{hv}}{}^* - S_{\mathrm{hv}} S_{\mathrm{vv}}{}^*) \rangle, \\
M_{34} &= -M_{43} = \langle \Im(S_{\mathrm{hh}} S_{\mathrm{vv}}{}^* + |S_{\mathrm{hv}}|^2) \rangle,
\end{aligned}
\tag{4}
$$

where $\langle \cdot \rangle$ is the ensemble average operator, * means the complex conjugate, and $\Re$ and $\Im$ stand for real and imaginary parts, respectively. The Mueller matrix representation is the most general representation of polarimetric scattering (Cloude 1986; Van Zyl, Papas, and Elachi 1987), and it has been demonstrated that there is a one-to-one mapping with other second-order scattering descriptors, i.e. **T** or **C**. The former matrix can be constructed from the target vector $\boldsymbol{k}$, which is obtained projecting the scattering matrix **S** onto the Pauli basis. In the backscattering case and assuming the reciprocity is satisfied, **T** is given by (Cloude and Pottier 1996)

$$
\mathbf{T} = \langle \boldsymbol{k}\boldsymbol{k}^{\dagger^{\mathrm{T}}} \rangle, \quad \boldsymbol{k} = \frac{1}{\sqrt{2}}[S_{hh} + S_{vv},\ S_{hh} - S_{vv},\ 2S_{hv}]^{\mathrm{T}}, \tag{5}
$$

where **T** stands for transpose and † means complex conjugate transpose. A formally equivalent representation is based on the covariance **C** matrix that is obtained projecting the scattering matrix onto the lexicographic basis (Cloude and Pottier 1996).

2.2. *Compact-polarimetry SAR architectures*

A CP SAR is a dual-polarimetric system that, in response to a $\pi/4$ or circular illumination, receives coherently according to an orthogonal basis. Typically the linear $\{h, v\}$ basis is adopted (Raney et al. 2011). When a circularly polarized wave is transmitted, the CP configuration is called hybrid-polarity (HP); while when a slant linearly polarized wave is transmitted it is called $\pi/4$ mode. In both cases, the received electric field can be written as

$$
\boldsymbol{E}_{\mathrm{r}} = \begin{pmatrix} E_{\mathrm{h}q} \\ E_{\mathrm{v}q} \end{pmatrix}, \tag{6}
$$

where q stands for the transmitted polarization that can be a right-/left-handed circular or a $\pi/4$ slant linear. To describe the polarimetric behaviour of the received wave, wave polarization theory must be adopted. Hence, the coherence matrix $\boldsymbol{\Gamma}$ must be used:

$$\mathbf{\Gamma} = \langle \boldsymbol{E}_{\mathrm{r}} \boldsymbol{E}_{\mathrm{r}}^{\dagger} \rangle = \begin{pmatrix} \langle E_{\mathrm{h}q} {E_{\mathrm{h}q}}^{*} \rangle & \langle E_{\mathrm{h}q} {E_{\mathrm{v}q}}^{*} \rangle \\ \langle E_{\mathrm{v}q} {E_{\mathrm{h}q}}^{*} \rangle & \langle E_{\mathrm{v}q} {E_{\mathrm{v}q}}^{*} \rangle \end{pmatrix} = \begin{pmatrix} \Gamma_{\mathrm{hh}} & \Gamma_{\mathrm{hv}} \\ \Gamma_{\mathrm{vh}} & \Gamma_{\mathrm{vv}} \end{pmatrix}. \tag{7}$$

An entirely equivalent approach consists of describing the polarization properties of the received field using the Stokes vector, that for a CP SAR system can be expressed as

$$\boldsymbol{s} = \left(\langle |E_{\mathrm{h}q}|^2 + |E_{\mathrm{v}q}|^2 \rangle,\ \langle |E_{\mathrm{h}q}|^2 - |E_{\mathrm{v}q}|^2 \rangle,\ 2\Re(\langle E_{\mathrm{h}q} {E_{\mathrm{v}q}}^{*} \rangle),\ -2\Im(\langle E_{\mathrm{h}q} {E_{\mathrm{v}q}}^{*} \rangle) \right)^{\mathrm{T}},\ \ {s_0}^2 \geq \sum_{i=1}^{3} {s_i}^2, \tag{8}$$

where the inequality expresses the partially polarized behaviour of the received wave. In Cloude, Goodenough, and Chen (2012), it was shown that the information content of CP measurements represents a consistent subset with respect to the one provided by quad-polarimetric SARs, and that in several applications the quad-polarimetric information can be preserved to obtain CP performance that tends to the quad-polarimetric ones.

3. Polarimetric SAR features

The set of polarimetric features that, based on either the Mueller matrix or the coherence matrix, is used for sea oil slick observation purposes is detailed here. The features are described according to the radar configuration that is exploited, i.e. quad-polarimetric, i.e. the full scattering matrix **S** of Equation (2) is needed, dual-polarimetric and CP features are specified.

3.1. Quad-polarimetric features

Quad-polarimetric features can be all obtained either by **M** or **T**. When the latter is adopted, the most common features are the ones arising by the eigenvalue/eigenvector decomposition (Cloude and Pottier 1996). Accordingly, under the reciprocity assumption, **T** can be uniquely decomposed into the sum of three deterministic scattering mechanisms, described by the eigenvectors $\boldsymbol{u}_i$, where their relative power is given by the eigenvalues λ_i (Cloude and Pottier 1996):

$$\mathbf{T} = \sum_{i=1}^{3} \lambda_i \boldsymbol{u}_i \boldsymbol{u}_i^{\dagger}. \tag{9}$$

Following this decomposition, some features can be defined (Lee and Pottier 2009). The scattering entropy H, defined from the logarithmic spectrum of the eigenvalues associated with **T**, is given by (Cloude and Pottier 1996)

$$H = -\sum_{i=1}^{3} p_i \log_3 p_i, \quad p_i = \frac{\lambda_i}{\sum_{i=1}^{3} \lambda_i}, \quad \lambda_1 \geq \lambda_2 \geq \lambda_3 \geq 0. \tag{10}$$

It is a basis-invariant measure of the degree of randomness of the polarimetric scattering behaviour that rules the observed scene. In fact, in Equation (10) each p_i represents the pseudo-probability associated with the ith independent, deterministic and

elementary polarimetric scattering mechanism described by the corresponding eigenvalue λ_i. As a matter of fact, since $0 \leq H \leq 1$, when H tends to 0 the imaged scene is characterized by a deterministic scattering, i.e. one dominant scattering mechanism, $\lambda_1 \neq 0, \lambda_2 = \lambda_3 = 0$. When H tends to 1, the scene is ruled by a completely depolarizing scattering, i.e. three coherent scattering mechanisms, $\lambda_1 = \lambda_2 = \lambda_3$. An alternative formulation of the Cloude–Pottier target entropy, $\hat{H}$, has been proposed by Praks, Koeniguer, and Hallikainen (2009). It is an approximated version of H that allows avoiding time-consuming eigenvectors and eigenvalues computations, achieving a fitting error of about 2% (Praks, Koeniguer, and Hallikainen 2009):

$$\hat{H} = 2.52 - 0.78 \log_3[\det(\mathbf{N} + 0.16\mathbf{I})], \tag{11}$$

where $\det(\cdot)$ stands for the determinant, and $\mathbf{N}$ and $\mathbf{I}$ are the power-normalized coherence and identity matrices, respectively. Slick-free sea surface scattering is well described by the almost deterministic single-reflection Bragg scattering model that calls for entropy values close to 0; while the strong departure which is in place when dealing with oil-covered sea surface results in a significantly random scattering mechanism that calls for larger entropy values. In addition, in Migliaccio et al. (2009) it was shown that, using H, oil lookalikes belonging to the class of weak-damping lookalikes can be discriminated from oil slicks.

The anisotropy coefficient A can be defined from the eigendecomposition of the coherence matrix $\mathbf{T}$ as (Lee and Pottier 2009)

$$A = \frac{\lambda_2 - \lambda_3}{\lambda_2 + \lambda_3}, \tag{12}$$

where A is bounded between 0 and 1. It is a roll-invariant parameter, complementary to H, which describes the relative weight of the two smallest eigenvalues of the Cloude–Pottier eigendecomposition. Nevertheless, it should be noted that the anisotropy coefficient can be also evaluated by considering the two largest eigenvalues instead of the smallest ones as in Equation (12). Since in the case of low entropy values, the two smallest eigenvalues are noisier, in Skrunes, Brekke, and Eltoft (2014) a modified anisotropy coefficient, A_{12}, has been proposed for oil spill detection purposes. It is defined as the ratio between the difference and the sum of the pseudo-probabilities corresponding to the first two eigenvalues (Equation (10)). A_{12} results in larger values (close to 1) over slick-free ocean surface and lower values (close to 0) over oil slicks.

The mean scattering angle $\bar{\alpha}$ can be defined from the eigenvalue decomposition:

$$\bar{\alpha} = \sum_{i=1}^{3} p_i \alpha_i, \quad 0^\circ \leq \alpha_i = \cos\left(|\boldsymbol{u}_i(1)|\right)^{-1} \leq 90^\circ, \tag{13}$$

where each α_i represents the phase related to each scattering mechanism. $\bar{\alpha}$ describes the scattering mechanism that characterizes the observed scene. Traditionally, $\bar{\alpha}$ is widely employed together with entropy and anisotropy for SAR polarimetry-based classification purposes (Cloude and Pottier 1997; Lee and Pottier 2009; Cloude 2009). Hence, two different behaviours in terms of $\bar{\alpha}$ characterize the ocean surface with and without oil slicks: mean scattering angle values lower than 45° are to be expected over slick-free sea surface since it calls for single-reflection Bragg scattering, while slick-covered sea is

expected to result into larger mean scattering angle values due to its departure from Bragg scattering.

Another **T**-based polarimetric parameter is the geometric intensity v (namely covariance scaling factor when expressed in terms of the covariance matrix **C**) given by (Skrunes, Brekke, and Eltoft 2014)

$$v = \det(\mathbf{T})^{\frac{1}{3}}. \tag{14}$$

Although v is mathematically similar to the span, i.e. the total backscattered power of the polarimetric scattering channels as well as the sum of the three eigenvalues of **T**, it is computed as the geometric mean of the eigenvalues rather than the sum, also including cross products. Due to the reduced ocean roughness applying over oil slicks, v calls for values lower than the ones of slick-free sea surface.

All those polarimetric features have been widely and successfully exploited for sea oil slick monitoring: the target entropy H in (Migliaccio, Gambardella, and Tranfaglia 2007; Nunziata, Gambardella, and Migliaccio 2012; Migliaccio, Nunziata, Montuori, et al. 2012), the anisotropy coefficient A and the mean scattering angle $\bar{\alpha}$ in (Zhang et al. 2011; Skrunes, Brekke, and Eltoft 2014) and the geometric mean or covariance scaling factor v in (Zhang et al. 2011; Skrunes, Brekke, and Eltoft 2014).

When the **M**-based approach is adopted, one can directly exploit the elements of the Mueller matrix (Equation (4)). Slick-free sea surface, being a reflection symmetric scene, results in a simplified Mueller matrix that contains only eight non-zero elements (Nghiem et al. 1992). In Nunziata, Gambardella, and Migliaccio (2008), the M_{33} element was exploited for sea oil slick observation purposes:

$$M_{33} = \langle \Re(S_{\mathrm{hh}} S_{\mathrm{vv}}{}^{*} + |S_{\mathrm{hv}}|^{2}) \rangle = M_{33}{}^{\mathrm{I}} + M_{33}{}^{\mathrm{II}}. \tag{15}$$

$M_{33}{}^{\mathrm{I}}$ is related to the correlation between co-polarized channels, which has been shown to be large when Bragg scattering applies (slick-free sea surface) and very low when a highly random scattering mechanism is in place (oil-covered sea surface). As a matter of fact, since $M_{33}{}^{\mathrm{II}}$ is low for both slick-free and oil slick-covered sea surface, a simple binary filter can be considered that, comparing $M_{33}{}^{\mathrm{I}}$ with $M_{33}{}^{\mathrm{II}}$, is able to distinguish oil slicks ($M_{33}{}^{\mathrm{I}} < M_{33}{}^{\mathrm{II}}$) from clean sea background ($M_{33}{}^{\mathrm{I}} > M_{33}{}^{\mathrm{II}}$). It was also demonstrated that a broad class of oil lookalikes, i.e. the one characterized by weak-damping properties, calls for a polarimetric behaviour indistinguishable from the sea surface one. Hence, this binary filter allows both observing sea oil slicks and distinguishing them from weak-damping lookalikes without any external threshold. Following a similar rationale, the conformity coefficient:

$$\mu = \frac{M_{44}}{M_{11}}. \tag{16}$$

can be defined. Even in this case, μ allows partitioning automatically the output space into two non-overlapping regions, i.e. slick-free or weak-damping slick-covered sea surface ($\mu > 0$) and oil slick-covered sea surface ($\mu < 0$). This approach was first used by (Zhang et al. 2011) for sea oil slick detection purposes.

Considering the approach that relies on the Mueller matrix, a basis-invariant parameter spanning from 0 to 1 can be straightforwardly defined from the Stokes vector of the

backscattered field $\boldsymbol{s}^{s}$ of Equation (3). It is the degree of polarization p, that measures how close the scattering mechanism of the observed scene is to be deterministic. It is given by (Lee and Pottier 2009)

$$p = \frac{\sqrt{\boldsymbol{s}^{s}(2) + \boldsymbol{s}^{s}(3) + \boldsymbol{s}^{s}(4)}}{\boldsymbol{s}^{s}(1)}. \tag{17}$$

Different formulations of p can be obtained based either on **T** and **M** (Sarabandi 1992; Gil 2000, 2007). p has been used in (Nunziata, Gambardella, and Migliaccio 2012; Nunziata, Migliaccio, and Li 2015) to both observe oil slicks and distinguish them from weak-damping lookalikes. In fact, when Bragg scattering applies, i.e. both over slick-free and weak-damping slick-covered sea surface, larger values are obtained (close to 1). When an oil slick is present, very low values (close to 0) are obtained due to the significant departure from Bragg scattering.

The polarization signature, which represents a 3-D plot of the power scattered off the scene when identical (co-polarized signature) or orthogonal (cross-polarized signature) transmitting/receiving antenna polarizations are used, has been widely employed for classification purposes. In Nunziata, Migliaccio, and Gambardella (2011), the pedestal on which the co-polarized signature is set has been shown to be a reliable estimator of the amount of unpolarized backscattered energy. Hence, the normalized pedestal height, P_{height}, has been used for sea oil slick observation purposes. The underpinning rationale relies on the fact that sea surface, being a Bragg scattering scene, results in a negligible P_{height} (close to 0). Significantly larger P_{height} values (close to 1) occur when an oil-covered sea surface is considered, due to the high scattering randomness of the oil-covered sea surface scattering. It must be noted that in Nunziata, Migliaccio, and Gambardella (2011) it was shown that oil lookalikes belonging to the class of weak-damping surfactants are indistinguishable from slick-free sea surface in terms of P_{height}. Hence, even P_{height} allows both observing oil slicks and discriminating them from weak-damping lookalikes.

All these polarimetric parameters have been widely and successfully employed to observe sea oil slicks: the M_{33}-based filter in Nunziata, Gambardella, and Migliaccio, (2008), the conformity parameter μ in Zhang et al. (2011), the degree of polarization p in Nunziata, Gambardella, and Migliaccio (2012, 2013), and the normalized pedestal height P_{height} in Nunziata, Migliaccio, and Gambardella (2011); Migliaccio et al. (2009); Nunziata, Gambardella, and Migliaccio (2012); Migliaccio and Nunziata (2014).

The quad-polarimetric features presented in this section are summarized in Table 2 together with their expected behaviour over slick-free or weak-damping slick-covered sea surface and oil-covered sea surface.

3.2. *Dual-polarimetric features*

In this section, the polarimetric features that can be obtained using a subset of the scattering matrix **S** (Equation (2)) are detailed.

The co-polarized phase difference ϕ, i.e. the phase difference between the co-polarized scattering amplitudes, is given by

$$\phi = \angle(S_{\text{hh}} S_{\text{vv}}^{*}), \tag{18}$$

Table 2. Most employed polarimetric features and their expected behaviour over sea surface with and without oil slicks.

Polarimetric feature	Slick-free sea surface/weak-damping lookalike	Oil slick-covered sea surface	References
H	Low	High	Migliaccio, Gambardella, and Tranfaglia (2007), Migliaccio, Nunziata, Montuori, et al. (2012), Minchew, Jones, and Holt (2012)
A	Low	High	Minchew, Jones, and Holt (2012), Skrunes, Brekke, and Eltoft (2014), Skrunes et al. (2014)
A_{12}	High	Low	Skrunes, Brekke, and Eltoft (2014)
$\bar{\alpha}$	Low	High	Minchew, Jones, and Holt (2012)
v	High	Low	Skrunes, Brekke, and Eltoft (2014), Skrunes et al. (2014)
M_{33}	$\lvert M_{33}{}^{\mathrm{I}}\rvert > M_{33}{}^{\mathrm{II}}$	$\lvert M_{33}{}^{\mathrm{I}}\rvert < M_{33}{}^{\mathrm{II}}$	Migliaccio et al. (2011), Skrunes et al. (2014)
μ	>0	<0	Zhang et al. (2011), Skrunes, Brekke, and Eltoft (2014), Skrunes et al. (2014)
p	High	Low	Shirvany, Chabert, and Tourneret (2012), Nunziata, Gambardella, and Migliaccio (2013)
P_{height}	Low	High	Nunziata, Migliaccio, and Gambardella (2011), Nunziata, Gambardella, and Migliaccio (2012)
σ_ϕ	Low	High	Migliaccio, Nunziata, and Gambardella (2009), Velotto et al. (2011), Nunziata, Migliaccio, and Gambardella (2011)
ρ_{co}	High	Low	Skrunes, Brekke, and Eltoft (2014)
P_{w}	High	Low	Shirvany, Chabert, and Tourneret (2012), Nunziata, Migliaccio, and Li (2015), Kumar, Kishore, and Rao (2014)
H_{w}	Low	High	Nunziata, Migliaccio, and Li (2015), Salberg, Rudjord, and Solberg (2014)
$\lvert\xi\rvert$	High	Low	Nunziata, Migliaccio, and Li (2015), Salberg, Rudjord, and Solberg (2014)
ϱ	High	Low	Nunziata, Migliaccio, and Li (2015), Salberg, Rudjord, and Solberg (2014), Yin et al. (forthcoming)
$\sin(2\chi)$	<0	>0	Kumar, Kishore, and Rao (2014), Salberg, Rudjord, and Solberg (2014), Li et al. (2015)
ζ	<1	>1	Nunziata, Migliaccio, and Li (2015), Salberg, Rudjord, and Solberg (2014)
μ_{HP}	>0	<0	Zhang et al. (2011), Nunziata, Migliaccio, and Li (2015), Salberg, Rudjord, and Solberg (2014)

Note: Note that for each feature some of the studies where the feature is proposed/used are referenced.

where the symbol $\angle$ means phase. ϕ has been widely used for classification purposes. The first application of the co-polarized phase difference for sea oil slick observation was proposed in Migliaccio, Nunziata, and Gambardella (2009), where a polarimetric scattering model was introduced to relate the ϕ standard deviation, σ_ϕ, to the departure from Bragg scattering. Accordingly, slick-free or weak-damping slick-covered sea surface call for low σ_ϕ values, while significantly larger σ_ϕ values result when oil-covered sea surface is considered.

Following a similar rationale, the modulus of the co-polarized complex correlation coefficient, ρ_{co}, has been used for sea oil slick monitoring purposes (Velotto et al. 2011; Skrunes, Brekke, and Eltoft 2014; Skrunes, Brekke, and Doulgeris 2015):

$$\rho_{co} = \left| \frac{\langle S_{hh} S_{vv}^{*} \rangle}{\sqrt{\langle |S_{hh}|^2 \rangle \langle |S_{vv}|^2 \rangle}} \right|. \tag{19}$$

It is a dual-polarimetric parameter that spans from 0 to 1. It is expected that ρ_{co} results in values close to 1 over slick-free sea surface due to its dominant Bragg scattering, while significantly lower ρ_{co} values, close to 0, are expected for oil-covered sea surface.

Note that, although σ_{ϕ} and ρ_{co} are considered dual-polarimetric features, they cannot be evaluated using standard products provided by conventional dual-polarimetric SAR (see Table 1). In fact, conventional dual-polarized SAR systems measure hh/hv or vv/vh polarimetric scattering channels combinations. The only exception is TerraSAR-X, the DLR X-band multi-polarization SAR, which provides routinely dual-polarized hh-vv stripmap and spotlight measurements. In addition, it must be noted that although dual-polarimetric hh-vv modes are implemented on Environmental Satellite (ENVISAT) advanced synthetic aperture radar (ASAR) and COSMO-SkyMed (see Table 1), they are incoherent SAR systems and thus they provide no phase information. When dealing with hh-hv or vv-vh dual-polarimetric SAR modes, the cross-polarized channel offers no polarimetric information useful for sea oil slick observation. Hence, for sea oil slick observation purposes such dual-polarized SARs behave as single-polarization systems since only the information carried on the co-polarized channels is useful. It must be pointed out that, with respect to the quad-polarimetric case, hh-vv dual-polarimetric measurements do not suffer from calibration issues and hh-vv dual-polarimetric features are not critically affected by the noise floor.

Nevertheless, the capability of all the abovementioned dual-polarimetric parameters to monitor sea oil pollution has been widely and successfully tested: σ_{ϕ} in Migliaccio, Nunziata, and Gambardella (2009); Nunziata, Gambardella, and Migliaccio (2012); Migliaccio et al. (2011); Skrunes, Brekke, and Eltoft (2014); Skrunes et al. (2014) and ρ_{co} in Velotto et al. (2011) and Skrunes, Brekke, and Eltoft (2014); Skrunes et al. (2014).

The dual-polarimetric features here defined are reported in Table 2 together with their expected behaviour over slick-free or weak-damping slick-covered sea surface and oil-covered sea surface.

3.3. *Compact-polarimetric features*

The key polarimetric features related to the scattered wave received by a CP SAR architecture are here presented. They can be equivalently derived from the coherence $\mathbf{\Gamma}$ matrix defined in Equation (7) or from the Stokes vector $\boldsymbol{s}$ of Equation (8). Due to the limited availability of actual reliable CP SAR measurements, wave polarimetry concepts have been exploited to emulate CP SAR data from actual fully polarimetric SAR measurements. Once CP measurements are emulated, it is possible to characterize the polarimetric behaviour of the wave scattered off the scene and received by the SAR antenna.

Two compact basis-invariant parameters, namely the wave degree of polarization P_w and the wave entropy H_w, can be used to describe the state of polarization of a generic partially polarized wave. They can be physically understood as a measure on how close the wave is to be fully polarized and how far the electric field is from being completely random, respectively. They are mathematically given by (Born and Wolf 1980; Mandel and Wolf 1995; Gil 2007):

$$P_w = \sqrt{1 - \frac{4\det(\mathbf{\Gamma})}{\mathrm{tr}(\mathbf{\Gamma})^2}} = \frac{1}{s_0}\sqrt{\sum_{i=1}^{3} {s_i}^2}, \tag{20}$$

$$H_w = -\mathrm{tr}(\hat{\mathbf{\Gamma}}\log_2\hat{\mathbf{\Gamma}}), \qquad \hat{\mathbf{\Gamma}} = \frac{\mathbf{\Gamma}}{\mathrm{tr}(\mathbf{\Gamma})}, \tag{21}$$

where $\mathrm{tr}(\cdot)$ stands for the trace operator. The wave degree of polarization P_w and the wave entropy H_w are both bounded in the interval [0, 1], where $P_w = 0$ ($H_w = 1$) means totally unpolarized wave and $P_w = 1$ ($H_w = 0$) stands for fully polarized wave. Hence, the received wave backscattered off a slick-free or a weak-damping surfactant-covered sea surface is expected to call for P_w (H_w) values close to 1 (0) since a deterministic Bragg scattering is in place; while the wave scattered off an oil slick results in significantly lower (larger) P_w (H_w) values.

The complex correlation coefficient ξ between the two orthogonal components of the received wave can be defined as (Born and Wolf 1980; Nunziata, Migliaccio, and Li 2015)

$$\xi = |\xi|e^{j\varrho} = \frac{s_2 + js_3}{\sqrt{s_0 + s_1}\sqrt{s_0 - s_1}}, \qquad \varrho = tg^{-1}\left(\frac{s_3}{s_2}\right), \tag{22}$$

where ϱ is the phase difference between the wave components along the v and h axes. Hence, a fully polarized wave is characterized by $|\xi| = 1$, while a totally unpolarized wave calls for $|\xi| = 0$. The wave scattered off a clean sea surface calls for $|\xi| = 1$ and ϱ values close to 90°, while the one backscattered from an oil-covered sea surface results in significantly lower $|\xi|$ and ϱ values, close to 0 and 0°, respectively.

In Salberg, Rudjord, and Solberg (2014), the ellipticity parameter has been employed as an indicator of the presence of a dominant Bragg scattering. It is defined as

$$\sin(2\chi) = -\frac{s_3}{ms_0}, \tag{23}$$

where χ is the ellipticity angle that varies in the range [–45°, +45°]. The sign of χ is related to the presence of odd- versus even-bounce backscattering, also in the case of transmitted field not perfectly circularly polarized. Slick-free sea surface calls for negative χ sign since Bragg scattering is a single-reflection mechanism. Mostly positive χ values are expected over oil-covered sea surface due to the randomness of the scattering mechanism (Salberg, Rudjord, and Solberg 2014). Hence, following this rationale, the ellipticity parameter allows obtaining a logical binary output in which Bragg and non-Bragg regions are clearly distinguished.

When considering the HP SAR architecture, to describe the polarization state of a randomly fluctuating wave backscattered off the observed scene, the circular polarization ratio ζ can be used (Raney et al. 2012; Shirvany, Chabert, and Tourneret 2012):

$$\zeta = \frac{\Gamma_{vv} + \Gamma_{hh} - 2\Im(\Gamma_{hv})}{\Gamma_{vv} + \Gamma_{hh} + 2\Im(\Gamma_{hv})}. \tag{24}$$

It is the ratio of the same-sense to opposite-sense circular polarization received power and allows measuring volumetric multiple scattering (Raney et al. 2012; Shirvany, Chabert, and Tourneret 2012). A low degree of circularity (<1) is to be expected for a wave scattered off a slick-free sea surface, while significantly larger ζ values apply for the one backscattered by an oil slick-covered sea surface (>1). This parameter has been firstly used in Nunziata, Migliaccio, and Li (2015), where it is shown to be able to observe oil slicks and distinguish them from weak-damping surfactants.

From HP SAR measurements the conformity coefficient μ_{HP} can be directly derived (Zhang et al. 2011):

$$\mu_{HP} = \frac{2(\Im(E_{hq}E_{vq}{}^{*}))}{(\langle|E_{hq}|^2\rangle + \langle|E_{vq}|^2\rangle)}. \tag{25}$$

It represents the HP version of the conformity parameter μ presented for conventional fully polarimetric SARs (see Equation (16)), thus having the same inherent ability to provide a binary output space in which it assumes positive values over sea surface or weak-damping surfactants, and negative values over oil slicks.

The capability of CP parameters to emphasize the presence of oil slicks over the sea background and to discriminate them from weak-damping lookalikes has been proved in different studies: the wave entropy H_w was used in Nunziata, Migliaccio, and Li (2015) the degree of polarization P_w in Shirvany, Chabert, and Tourneret (2012); Kumar, Kishore, and Rao (2014); Nunziata, Migliaccio, and Li (2015); Salberg, Rudjord, and Solberg (2014), the ellipticity parameter $\sin(2\chi)$ in Kumar, Kishore, and Rao (2014); Salberg, Rudjord, and Solberg (2014), the complex correlation coefficient ξ in Kumar, Kishore, and Rao (2014); Nunziata, Migliaccio, and Li (2015); Salberg, Rudjord, and Solberg (2014), the circular polarization ratio ζ in Nunziata, Migliaccio, and Li (2015), and the conformity index μ_{HP} in Salberg, Rudjord, and Solberg (2014).

It must be noted that, as well as hh-vv dual-polarimetric features, CP features are not affected by the hv channel limitation in terms of noise floor.

The expected behaviour over slick-free or weak-damping slick-covered sea surface and oil-covered sea surface of the compact-polarimetric features presented is summarized in Table 2.

4. Experiments and discussion

In this section, some thought experiments are presented to discuss the performance of the polarimetric features in observing sea oil slicks. The polarimetric features are presented according to the set of polarimetric data they need. First quad-polarimetric features are presented, then dual-polarimetric ones and finally CP features. The description is aimed at witnessing the peculiar benefits of each polarimetric feature for sea oil slick observation according to end-users needs, i.e. oil detection and oil characterization.

4.1. Data sets

In this section, the SAR data set is presented. It consists of four fully polarimetric single-look complex (SLC) spaceborne SAR data collected by ALOS PALSAR and Radarsat-2 (see Table 1), where well-known oil slicks and weak-damping lookalikes are present. In addition, to demonstrate the ability of polarimetric approaches to provide at least rough information on the damping properties of the detected oil slicks, a fully polarimetric multi-look complex (MLC) airborne L-band UAVSAR acquisition is considered. This is due to the fact that this kind of information is particularly useful for remediation purposes in the case of large accidental oil spills. Hence, from an operational viewpoint, a dedicated observation should be preferred.

In Figure 1(*a*), an excerpt of the vv-polarized intensity image relevant to the ALOS-PALSAR acquisition (ID: ALPSRP031440190) collected on 27 August 2006 off Guimaras Island, in the Philippines, is shown as grey-tone image. The heavy oil slick due to the Solar 1 accident is clearly visible as a dark patch (Migliaccio et al. 2009; Nunziata, Gambardella, and Migliaccio 2012). In Figure 1(*b*), an excerpt of the vv-polarized intensity image relevant to the ALOS-PALSAR acquisition, where a well-known weak-damping lookalike is present, is shown (Migliaccio et al. 2009). This SAR data was collected off the coast of Dá Nang (Vietnam) on 10 March 2007 (ID: ALPSRP059890330). The vv-polarized intensity image relevant to the Radarsat-2 acquisition (ID: PDS_01141690) collected on 15 May 2010 off the Louisiana Coasts, in the Gulf of Mexico, is shown in Figure 1(*c*). The imaged area covers a well-known oil field where both metallic targets and oil slicks are present (Migliaccio, Nunziata, Montuori, et al. 2012). In Figure 1(*d*), an excerpt of the vv-polarized intensity image relevant to the Radarsat-2 acquisition of the 14 December 2009 (ID: PDS_00886040), collected off the coast of California, is shown. A certified weak-damping lookalike due to the produced-water discharge of an oil rig, clearly visible in the centre of the image, can be noted. Figure 1(*e*) shows an excerpt of the vv-polarized intensity image related to the UAVSAR acquisition of 23 June 2010 that imaged the large Deepwater Horizon accident area (ID: 14010) (Migliaccio and Nunziata 2014).

4.2. Quad-polarimetric experiments

In this section, experiments undertaken using quad-polarimetric features are presented and discussed. Following the theoretical rationale described in Section 3, quad-polarimetric features can be sorted out into two classes. The first one includes features which allow obtaining a logical binary output where heavy-damping oils are clearly distinguished from both the surrounding sea and weak-damping lookalikes without any external threshold, i.e. the M_{33}-based filter and the μ approach. The second class includes features that allow emphasizing (de-emphasizing) oil slicks (weak-damping surfactants) with respect to the sea background, e.g. H, P_{height}, p, etc.

With respect to the first class, as a showcase, we applied the μ approach to the polarimetric data of Figures 1(*a*) and (*b*). The output of the μ filter is shown in Figures 2 (*a*) and (*b*), where one can easily note that the dark areas of Figures 1(*a*) and (*b*) are due to completely different phenomena. The former one is due to a surfactant whose damping properties are strong enough to result in a non-Bragg scattering that can be easily separated for the Bragg scattering that characterizes the surrounding slick-free sea surface, i.e. an oil slick. The latter dark area is due to a surfactant that, although resulting in a backscattered signal lower than the surrounding sea (see dark area in

Figure 1(*b*)), does not call for damping properties strong enough to led to a non-Bragg scattering. Therefore, this surfactant is indistinguishable from the surrounding sea surface in terms of polarimetric scattering features. It can be noted that both the binary outputs have been obtained without any external threshold. Hence, this makes this method very attractive operationally when the focus is the detection and discrimination. Similar results, not shown to save space, can be obtained using the M_{33} approach (Nunziata, Gambardella, and Migliaccio 2008; Migliaccio et al. 2009).

With respect to the second class, as showcase, we applied H to the polarimetric measurements of Figures 1(*c*) and (*d*). The output is shown in Figures 2(*c*) and (*d*),

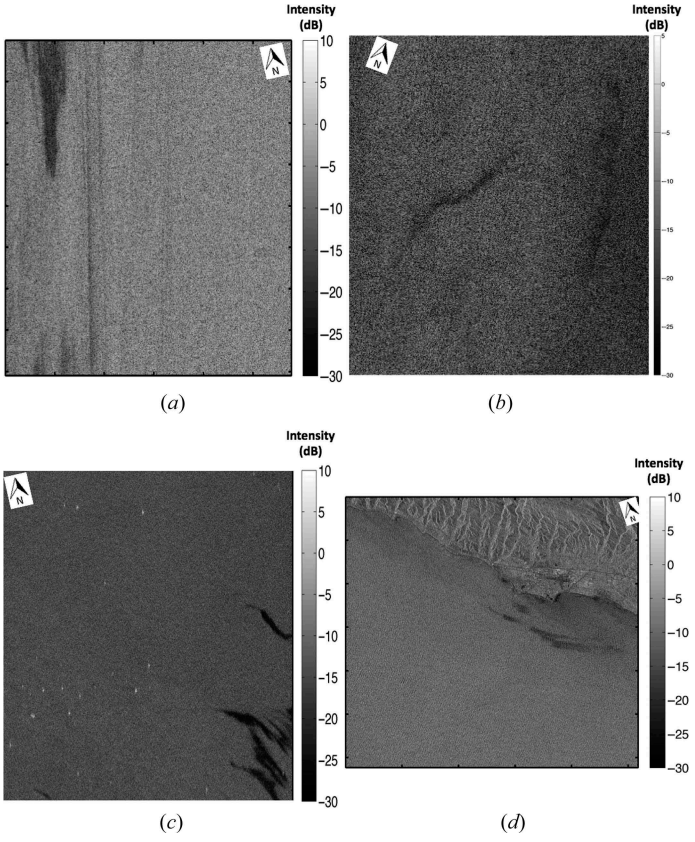

Figure 1. Polarimetric data set. (*a*) Excerpt (5.405 km × 3.059 km) of the vv-squared modulus image (dB) relevant to the ALOS-PALSAR data collected on 27 August 2006 off Guimaras Island, Philippines (centre image coordinates 10° 15′ N, 122° 29′ E), where a certified heavy oil slick is present. (*b*) Excerpt (3.757 km × 1.342 km) of the vv-squared modulus image (dB) relevant to the ALOS-PALSAR data collected in Vietnam, off the coast of Dá Nang (centre image coordinates 16° 42′ N, 108° 22′ E), on 10 March 2007, where a well-known weak-damping lookalike is visible. (*c*) Excerpt ($\approx$ 16 km × 11 km) of the vv-squared modulus image (dB) relevant to the Radarsat-2 data collected on 15 May 2010 off the Louisiana Coasts, in the Gulf of Mexico (centre image coordinates 29° 34′ N, 89° 45′ W), where few oil slicks and metallic targets (likely due to oil rigs) are present. (*d*) vv intensity image (dB) relevant to the Radarsat-2 image acquired off the coast of California on 14 December 2009 (29.478 km × 12.168 km), where a weak-damping lookalike due to an oil rig produced-water discharge is present. (*e*) Excerpt ($\approx$ 60 km × 14 km) of the vv-squared modulus image (dB) relevant to the UAVSAR acquisition of 23 June 2010 collected during the Deepwater Horizon accidental oil spill (centre image coordinates 29° 18′ N, 88° 57′ W).

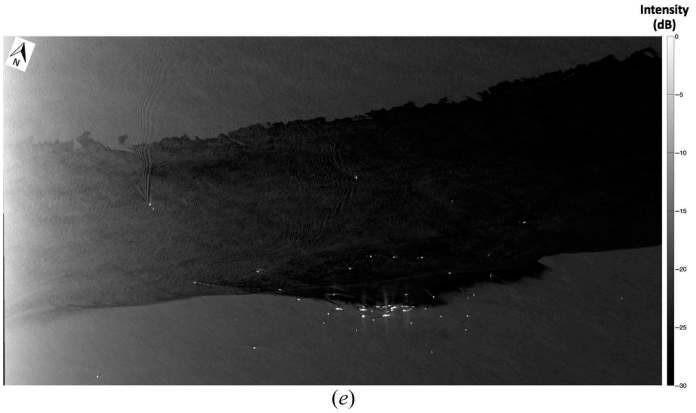

(*e*)

Figure 1. (*Continued*).

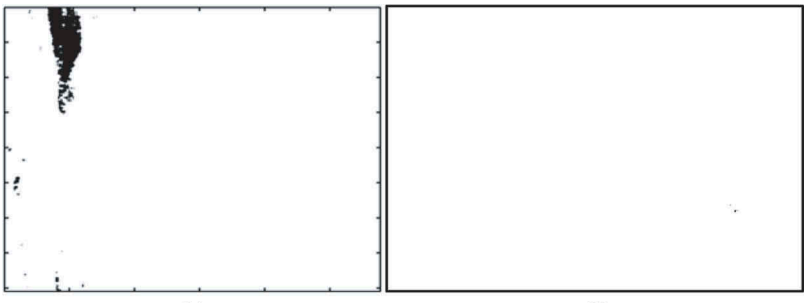

(*a*) (*b*)

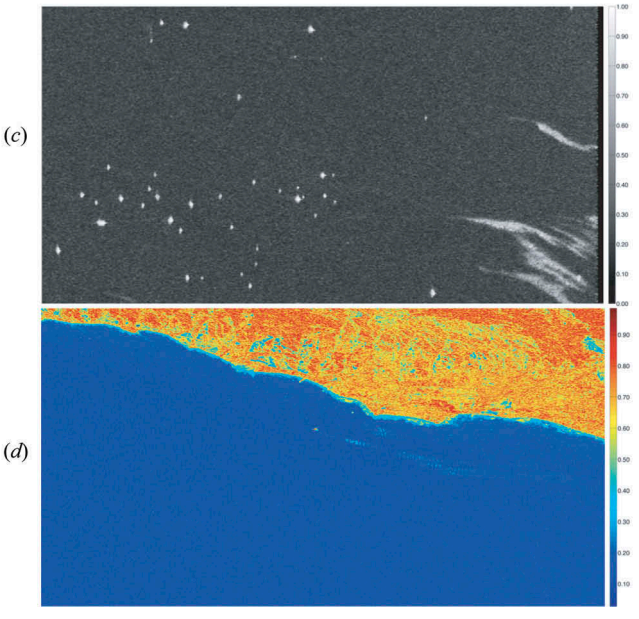

(*c*)

(*d*)

Figure 2. Sea oil slick observation by quad-polarimetric SAR features. μ binary mask related to (*a*) the scene of Figure 1(*a*); (*b*) the scene of Figure 1(*b*). H image related to (*c*) the scene of Figure 1(*c*); (*d*) the scene of Figure 1(*d*).

where one can easily note that, even in this case, oil slicks (Figure 2(*c*)) can be straightforwardly distinguished from both the surrounding sea and the weak-damping lookalike (Figure 2(*d*)). Oil slicks result in a significant departure from the sea surface Bragg scattering as one can note by the oil and sea H values, ≈ 0.9 and ≈ 0.2, respectively. This implies that H allows emphasizing the oil slick with respect to the surrounding sea. Note also that metallic targets result in a behaviour similar to the oil one. On the other side, the lookalike of Figure 1(*d*), although resulting in a lower backscattered signal in the intensity image, calls for a negligible departure from the sea surface Bragg scattering. Hence, the lookalike is indistinguishable from the surrounding sea in terms of H (both call for H values close to 0.3). This implies that the lookalike is de-emphasized with respect to the surrounding sea if compared to the single-polarization image. Similar results can be obtained considering all the quad-polarimetric features belonging to this class. A fair ranking of the features' performance in terms of oil/sea contrast has been proposed in Nunziata, Gambardella, and Migliaccio (2013), where it has been shown that P_{height} performs best. Note that all the polarimetric features belonging to this class need an external threshold to provide a logical binary output. This threshold can be set either globally or in an adaptive way. Note also that results shown in Figures 2(*a*)–(*d*) have been obtained processing SAR data collected over completely different areas by SARs operating at different frequencies. This witnesses the robustness of the polarimetric approaches.

All quad-polarimetric features allow measuring the departure from Bragg scattering. Hence, one may think to exploit this capability to obtain rough information on the spatial variability in terms of damping properties to characterize a given surfactant. This is a topic of paramount interest for example when dealing with remediation activities as it has recently been shown in several studies related to both the Deepwater Horizon accident (Jones et al. 2011; Migliaccio et al. 2011; Minchew, Jones, and Holt 2012; Collins et al. 2015) and a controlled oil spill experiment (Skrunes, Brekke, and Eltoft 2014; Skrunes et al. 2014). As a showcase, we describe the main outcomes obtained in Migliaccio and Nunziata (2014), where P_{height} was applied to the airborne UAVSAR data collected over the surfactant related to the Deepwater Horizon accident (see Figure 1(*e*)). The output is shown in Figure 3(*a*), where the P_{height} image is presented. Analysing deeply P_{height} values over the whole slick-covered area one may note that they are compatible with a Bragg-type scattering mechanism. This implies that a weak-damping surfactant is in place. In fact, in Migliaccio et al. (2009), it was shown that within the considered area, corresponding to the huge Deepwater Horizon accidental oil spill, the dominant scattering mechanism, both over the slick-free and the slick-covered sea surface, was the Bragg one. This unconventional result can be physically understood considering that: (1) the spilled oil was a 'light oil'; (2) a large use of dispersant was made to mitigate pollution effects, generating a complex oil-water chemical mixture; (3) the released oil was coming from the bottom of the sea. Incidentally, note that in such a case the standard single-polarization SAR oil slick monitoring procedures are not effective. In addition, Figure 3(*a*) clearly shows a spatial variability of P_{height} within the slick-covered area. This implies that the amount of unpolarized backscattered energy is varying spatially and, therefore, the damping properties of the pollutant are not homogeneous. To unambiguously map the damping properties of the pollutant, an unsupervised k-means clustering method is applied to the P_{height} output that results in the image shown in Figure 3(*b*). Four classes that correspond to different polarimetric scattering properties are visible. From the left-side of the image one can find: (1) a 'red strip' calling for negligible P_{height} values (<0.025). This implies that specular reflection applies in this area due to very low

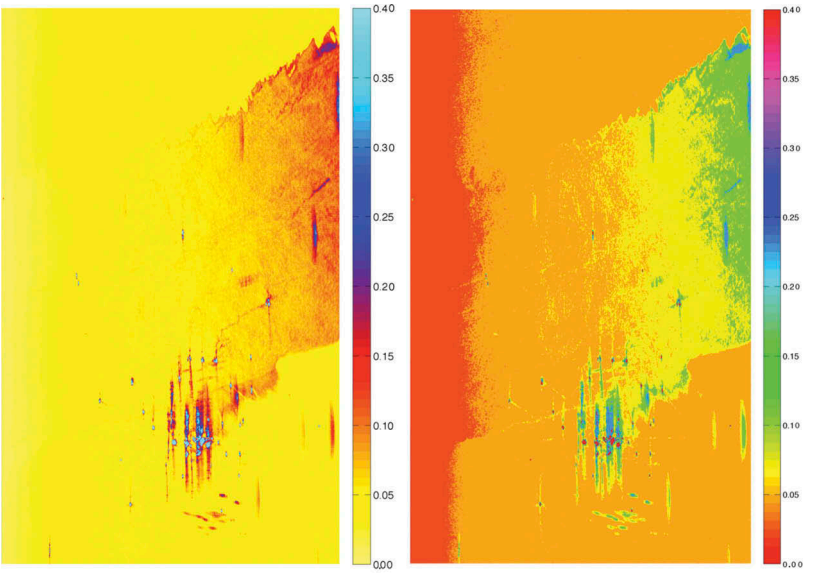

Figure 3. Sea oil slick observation by quad-polarimetric SAR features. (*a*) P_{height} output related to the scene of Figure 1(*e*); (*b*) output of the 4-classes k-means partitioning algorithm applied to the P_{height} output.

incidence angles (Migliaccio and Nunziata 2014). In fact, UAVSAR look angle varies from 22° (near range) to 65° (far range). (2) An 'orange area', that calls $P_{\text{height}} \approx 0.05$. Note that this area includes both slick-covered and slick-free sea surface. This implies that the surfactant belonging to this area is characterized by very low damping properties (e.g. thin sheen layers, wake-induced features, etc.). This result has been confirmed by helicopter photos (Migliaccio and Nunziata 2014). (3) A 'yellow area', that calls for a non-negligible amount of unpolarized energy witnessing that a surfactant characterized by stronger damping properties is present. This result is confirmed by aerial and helicopter observations (Migliaccio and Nunziata 2014). (4) A 'green area' calling for the largest unpolarized backscattered energy ($P_{\text{height}} > 0.1$). This implies that a surfactant with stronger damping properties is present (on the right-hand side of the rig site related to the bright blue spots in the bottom centre of Figure 3(*a*)). However, the large amount of unpolarized energy on the right-hand side of the image is probably due to the noise that affects the hv channel at incidence angles larger than $\approx 55°$. In fact, for incidence angles above $\approx 55°$ the hv channel is practically uninformative as it was pointed out in Jones et al. (2011). This implies that, although the detection is always possible since the noisy pixels belonging to the polluted area concur in a better definition of the oil slick (detection), the classification is less reliable.

In Minchew (2012), the same data set is analysed using both intensity-related features and polarimetric features derived from the eigenvalue/eigenvector decomposition. Polarimetric analysis shows results similar to the P_{height} ones, witnessing that a weak-damping surfactant is everywhere in place whose damping properties are spatially variant. In addition, considering only pixels above noise floor, it was shown that H and $\bar{\alpha}$ values are consistent with a Bragg scattering over both the oil slick-covered and slick-free sea

Table 3. SAR-based sea oil slick observation: performance according to user needs.

SAR architecture	Detection without external threshold	Oil/lookalike discrimination	Characterization
Fully polarimetric	M_{33}, μ	H, A, A_{12}, M_{33}, μ, p, P_{height}	P_{height}, H, A, $\bar{\alpha}$
Dual-polarimetric hh/vv	Not possible	σ_ϕ, $M_{33}{}^{\text{I}}$, ν	σ_ϕ, $M_{33}{}^{\text{I}}$, ν
Dual-polarimetric hh/hv, vv/vh	Not possible	Not possible	Not possible
Compact-polarimetric	$\sin(2\chi)$, μ_{HP}	P_{w}, H_{w}, $\sin(2\chi)$, μ_{HP}	P_w, H_{w}, ϱ, $\lvert\xi\rvert$
Single-polarization	Not possible	Not possible	Not possible

surface, while A shows significant spatial variations across the slick being more sensitive to the incidence angle. It is also shown that the change in backscatter within the polluted area was jointly due to both the damping of Bragg waves and a reduction of the effective dielectric constant of the surface. They estimated that the upper layer of the slick consists of a mixture composed by $\approx 80\%$ oil and $\approx 20\%$ water. Similar results have been found in Collins et al. (2015).

Experimental results referring to the capability of quad-polarimetric features to automatically detect oil slicks, to discriminate them from the broad class of weak-damping lookalikes, and to provide in-depth information on the damping properties of a given surfactant, are summarized in Table 3.

4.3. *Dual-polarimetric hh-vv experiments*

In this section, following the theoretical rationale described in Section 3, experiments undertaken using dual-polarimetric hh-vv features are presented and discussed. They are all able to emphasize (de-emphasize) the presence of oil slicks (weak-damping lookalikes) with respect to the surrounding sea, i.e. σ_ϕ and ρ_{co}. However, despite of the quad-polarimetric case, there is no dual-polarimetric feature that allows obtaining automatically a logical binary output without any external threshold. Hence, they all belong to the second class and thresholding algorithms have to be employed to perform oil slick detection.

As a showcase, we applied σ_ϕ to the SAR data set shown in Figures 1(*a*)–(*d*). Experimental results are shown in Figures 4(*a*)–(*d*), respectively. By looking at Figure 4(*a*) and (*c*), where well-known oil slicks are present, it is clear that σ_ϕ allows emphasizing the presence of oil slicks with respect to the surrounding sea since over oil slicks, as well as over man-made metallic targets, σ_ϕ calls for values ($>\approx 90^\circ$) significantly larger than the ones characterizing slick-free sea surface ($<\approx 50^\circ$). Results related to the certified weak-damping lookalikes of Figures 1(*b*) and (*d*) are shown in Figure 4(*b*) and (*d*), respectively. In both cases, the weak-damping surfactant is de-emphasized, in terms of σ_ϕ, with respect to the surrounding sea. This is due to the fact that, since σ_ϕ is a measure of the departure from Bragg scattering, over weak-damping oil slicks a Bragg mechanism is still in place. In both cases, the weak-damping surfactant calls for σ_ϕ values $\approx= 50^\circ$. This implies that it is practically indistinguishable from the surrounding sea in terms of Bragg scattering. In Nunziata, Gambardella, and Migliaccio (2013), it was demonstrated that σ_ϕ achieves performance similar to quad-polarimetric features, i.e. P_{height} and p, in terms of de-emphasization of sweak-damping

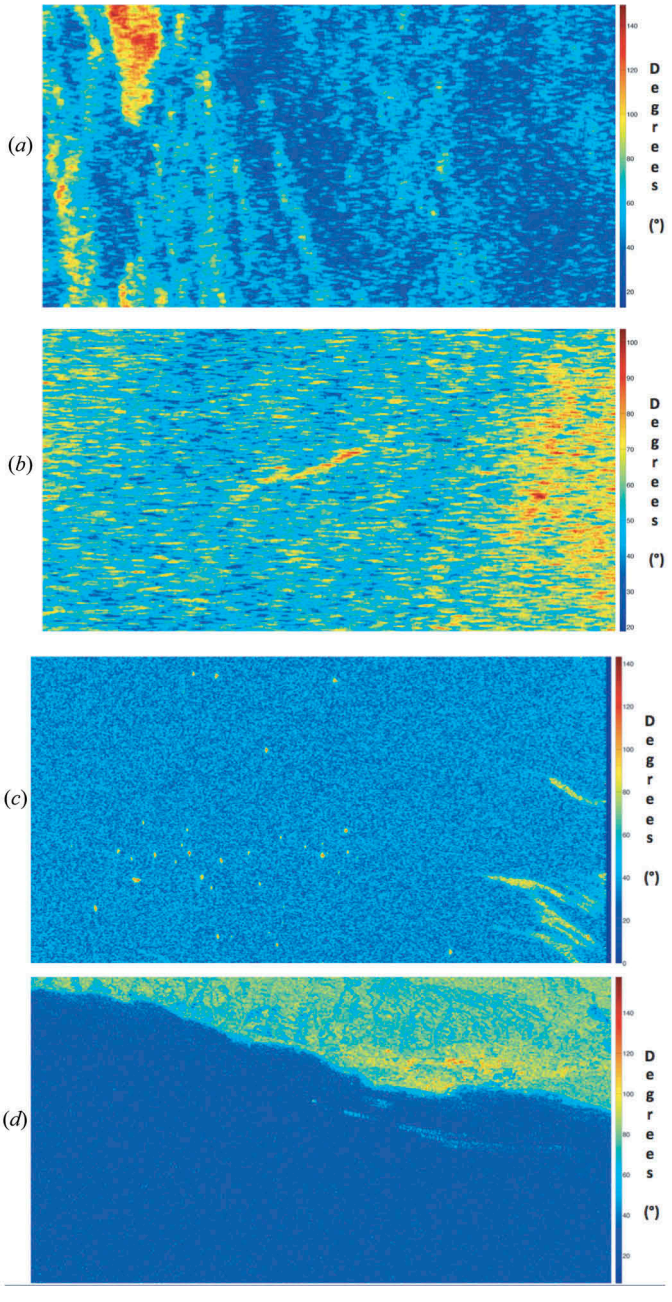

Figure 4. Sea oil slick observation by dual-polarimetric SAR features. (*a*) σ_ϕ image related to (*a*) the scene of Figure 1(*a*); (*b*) the scene of Figure 1(*b*); (*c*) the scene of Figure 1(*c*); (*d*) the scene of Figure 1(*d*).

surfactants, and that it was more effective from a processing time viewpoint. Similar results, not shown to save space, can be obtained using ρ_{co} (Skrunes, Brekke, and Eltoft 2014; Skrunes, Brekke, and Doulgeris 2015).

In Skrunes, Brekke, and Eltoft (2014), Skrunes et al. (2014), the capability of dual-polarimetric hh-vv features to provide rough information on the spatial variability of the damping properties within a given surfactant is analysed. A polarimetric SAR data set including both fully polarimetric Radarsat-2 and dual-polarimetric hh-vv TerraSAR-X acquisitions is considered. The data set is related to an oil-on-water exercise undertaken by the Norwegian Clean Seas Association for Operating Companies (NOFO) in the North Sea, in June 2011 and 2012. During these controlled experiments, oils characterized by different chemical/physical properties have been released into the sea. They include plant oil (Radiagreen ebo), emulsion oil (Oseberg blend) and crude oil (evaporated Balder), which differ in terms of viscosity, density, and volume. More detailed information on composition and properties of the released oils can be found in Skrunes, Brekke, and Eltoft (2014); Skrunes et al. (2014). In addition, the considered data set includes some lookalikes mostly due to natural phenomena. Nonetheless, it can be noted that the kind of plant oil considered in these experiments is expected to behave as a thin biogenic film (Gade, Huhnerfuss, and Korenowski 2006). When dealing with oil characterization, i.e. oil/lookalike discrimination and oil slick properties extraction, the hv channel can be severely affected by noise if low backscattering areas call for a signal below the instrument noise floor. This was the case of Radarsat-2 SAR data and, therefore, only the subset composed by the co-polarized hh and vv channels is considered for processing (Skrunes, Brekke, and Eltoft 2014; Skrunes et al. 2014). In Skrunes, Brekke, and Eltoft (2014), a large set of dual-polarimetric hh-vv features is investigated in terms of sea oil slick observation purposes. It includes σ_ϕ, ρ_{co}, M_{33}^{I} (Equation (15)), v, and the eigenvector/eigenvalue-based features obtained considering a 2×2 coherence matrix, i.e. $\mathbf{T}$ computed from the co-polarized channels. Dual-polarimetric features are shown to emphasize emulsion/crude oil with respect to the surrounding sea and to de-emphasize plant oil. An oil characterization is also undertaken demonstrating a good ability of all the features in showing a certain spatial variability of the surfactants' damping properties. In addition, a ranking of the dual-polarimetric features is also undertaken according to the oil/plant oil-sea contrast. It is shown that M_{33}^{I} and v perform the best in terms of emphasizing/de-emphasizing capabilities. In Skrunes et al. (2014), the same oil experiment is analysed including a TerraSAR-X data set. The analysis is undertaken using M_{33}^{I} and v, and log-cumulants. The results show that the best emphasizing/de-emphasizing capability is provided by Radarsat-2 although among them no one has to be preferred in terms of data quality.

To summarize, dual-polarimetric hh-vv experimental results are shown in Table 3, where their capability to perform oil characterization is synthetically reported.

4.4. *Compact-polarimetric experiments*

In this section, experiments undertaken using HP SAR data emulated from actual fully polarimetric SAR measurements are presented and discussed. As well as for quad-polarimetric features, following the theoretical rationale described in Section 3, CP features can be sorted out into two classes. The first class involves features which are able to provide automatically a logical binary output where oil slicks are clearly separated from both the surrounding sea and weak-damping lookalikes without any external threshold, i.e. the $\sin(2\chi)$ approach and the μ_{HP} filter. The second class includes features that allow emphasizing (de-emphasizing) oil slicks (weak-damping surfactants) with respect to the surrounding sea, e.g. the wave entropy H_w, the wave degree of polarization P_w, the circular polarization ration ζ, etc.

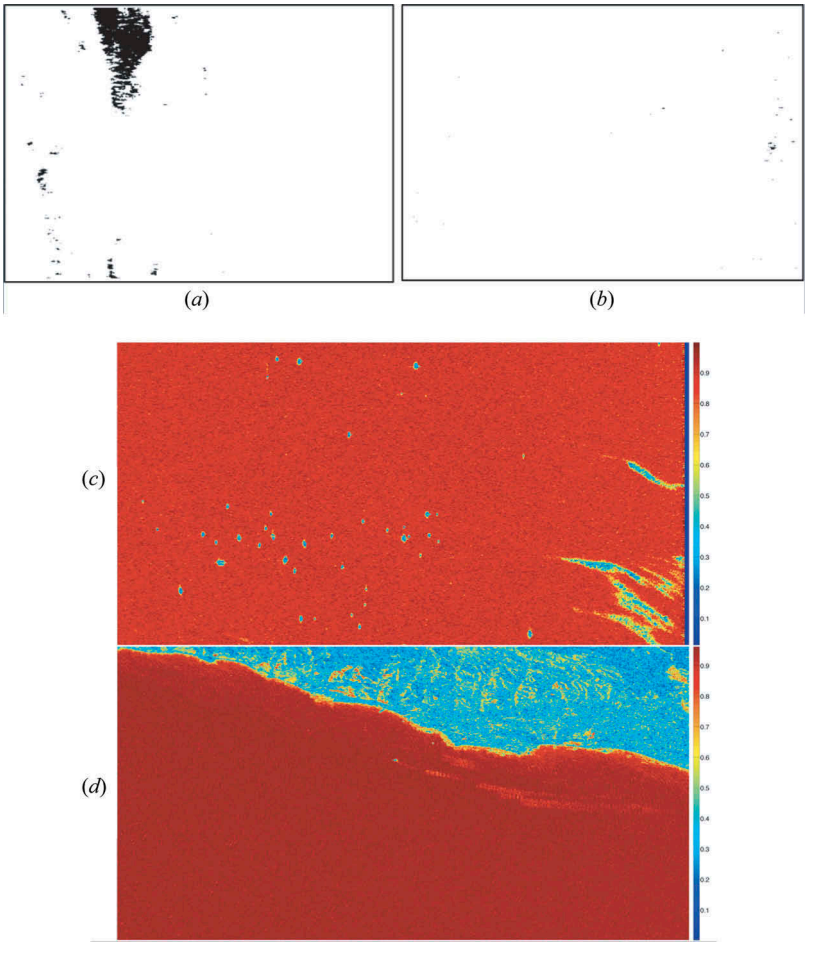

Figure 5. Sea oil slick observation by compact-polarimetric SAR features. $\sin(2\chi)$ binary mask related to (*a*) the scene of Figure 1(*a*); (*b*) the scene of Figure 1(*b*). P_w image related to (*c*) the scene of Figure 1(*c*); (*d*) the scene of Figure 1(*d*).

With respect to the first class, as a showcase, we applied the $\sin(2\chi)$-based filter to the polarimetric data set of Figures 1(*a*)–(*d*). The logical binary outputs are shown in Figures 5(*a*) and (*b*). As shown in Figure 5(*a*), Bragg scattering is everywhere in place but within the oil-covered area; hence, the scattered wave is almost fully polarized everywhere but within the oil slick. When dealing with a weak-damping surfactant, Bragg scattering applies everywhere, even within the dark areas of Figure 1(*b*), as shown in Figure 5(*b*). This implies that the backscattered wave is everywhere almost fully polarized. Hence, $\sin(2\chi)$) allows automatically observing sea oil slicks and distinguishing them from weak-damping lookalikes. Similar results, not shown to save space, are obtained processing SAR data shown in Figures 1(*c*) and (*d*), and employing the μ_{HP} approach.

With respect to the second class, as a showcase, we applied the wave degree of polarization P_w to the polarimetric SAR data of Figures 1(*c*) and (*d*). By looking at Figure 5(*c*) one can note that P_w is able to emphasize the presence of both oil slicks and

metallic targets with respect to the sea background. As expected, the wave scattered off the slick-free sea surface calls for large P_w values ($P_w \approx 0.9$) due to the dominant almost deterministic Bragg scattering, while oil-covered sea surface results in a backscattered wave calling for significantly lower values ($P_w \approx 0.4$). On the other side, Figure 5(*d*) clearly witnesses that the weak-damping lookalike results in a backscattered wave characterized by P_w values similar to the sea ones ($P_w \approx 0.8$). Hence, in this case, the weak-damping surfactant is de-emphasized since it results to be indistinguishable from the surrounding sea. Note that in both cases an adaptive or global external threshold has to be set in order to obtain a logical binary output. Similar results are obtained in Shirvany, Chabert, and Tourneret (2012), where P_w was used to emphasize the presence of oil spills with respect to the surrounding sea. Emulated HP and $\pi/4$ CP SAR data obtained from actual fully polarized L-band airborne (UAVSAR) and C-band spaceborne (Radarsat-2) SAR acquisitions are considered. However, similar results can be obtained using other CP features, i.e. H_w, ζ, $|\xi|$.

In Yin et al. (forthcoming), actual fully polarimetric C-band SAR data have been used to emulate CP architectures for sea oil slick observation. It was shown that oil slick detection and discrimination from typical oil lookalikes (i.e. biogenic surfactants) can be successfully performed interpreting polarimetric features within an extended version of the sea surface Bragg scattering model. It was shown that CP SAR architectures achieve results very similar to the one obtained from fully polarimetric SAR, and therefore that the HP mode is more suitable for sea oil slick observation than the $\pi/4$ configuration. In Nunziata, Migliaccio, and Li (2015), several HP features have been extracted from the coherence matrix $\mathbf{\Gamma}$ of HP SAR data emulated from actual L- and C-band fully polarimetric acquisitions to demonstrate the capability of the HP SAR architecture to detect oil slicks and distinguish them from weak-damping lookalikes. In Salberg, Rudjord, and Solberg (2014), a large set of CP features have been emulated from Radarsat-2 SAR data and employed to enhance oil spill detection performance and to discriminate between low-wind areas and oil slicks. It was shown that also CP features as ξ and the standard deviation of ϱ allow emphasizing the presence of sea oil slicks with respect to the surrounding sea and to distinguish low-wind areas from oil slicks. In addition, it was demonstrated that the $P_w - \chi$ decomposition is able to provide an oil/sea contrast better than the single CP feature, enhancing detection performance. In Li et al. (2015), the χ approach is used as an estimator of the different oil slick and sea surface scattering properties. It was shown that, in the case of the Deepwater Horizon accidental oil spill, χ exhibits the same behaviour over the polluted area and on the slick-free sea surface i.e. it assumes negative values. This is due to the fact that the single-bounce Bragg scattering was everywhere in place. In Kumar, Kishore, and Rao (2014), actual C-band HP SAR acquisitions collected by Risat-1 have been used to accomplish an unsupervised oil slick classifier that, based on both the $P_w - \chi$ and $P_w - \delta$ decompositions, allows detecting oil slicks and distinguishing them from weak-damping lookalikes. Note that this method is shown to be robust even when the transmitted field is not perfectly circularly polarized. To summarize, experimental results related to CP features are reported in Table 3, where their capability to automatically detect oil slicks and discriminate them from weak-damping lookalikes, and to provide at least rough information on the damping properties within a given slick is synthetized.

To analyse the capability of different HP features to perform sea oil slick detection and discrimination a mean contrast parameter can be considered. A fair ranking can be drawn for the following set of features: H_w, P_w, $|\zeta|$, $|\sin(2\chi)|$, and $|\mu_{HP}|$. This is due to the fact that they are all bounded between 0 and 1. Hence, their behaviour over slick-free, oil

slick-covered, and weak-damping lookalike covered sea surface samples is evaluated. The ranking is performed evaluating, for each feature, the mean oil/sea contrast over two equal-size regions of interest belonging to oil/lookalike and sea to assess the detection capability. The same approach is followed to evaluate the mean lookalike/sea contrast that is useful to assess the discrimination capabilities. When dealing with oil slick detection, a high mean oil/sea contrast is desired. Hence, according to this rationale, the HP feature that has shown the largest contrast is $|\mu_{HP}|$ (3.2709), while the lowest is achieved by $|\zeta|$ and $|\sin(2\chi)|$ ($\approx$ 1.2). H_w and P_w call for intermediate values of the mean oil/sea contrast. In the case of oil discrimination, a unitary value of the weak-damping lookalike/sea surface mean contrast witnesses that the surfactant behaves as slick-free sea surface in terms of scattering, thus the larger is the departure the poorer is the feature performance. Accordingly, experimental results show that $|\sin(2\chi)|$ performs best, achieving a mean lookalike/sea contrast close to 1 (1.0018), while H_w calls for the worst mean contrast (1.6533). All the other HP features exhibit performance very close to 1 ($\pm$ 5%).

As a general comment we can say that for oil spill observation purposes CP features perform well as far as the quad-polarimetric ones. However, since CP SAR architectures are able to observe areas significantly larger than the one imaged by a conventional fully polarimetric SAR system, they are operationally more attractive and they should be preferred. However, on the operational side it is important to analyse the SAR calibration issue on real data (Touzi et al. 1993; Touzi, Vachon, and Wolfe 2010).

Experimental results referring to the capability of polarimetric features to automatically detect oil slicks, discriminate them from the broad class of weak-damping lookalikes and to provide in-depth information on the damping properties of a given surfactant are summarized in Table 3.

5. Conclusions

In this review, the most up-to-date polarimetric SAR-based approaches for sea oil slick observation are presented and critically discussed. The topic has a relevant scientific and environmental importance. The monitoring of sea oil slicks is addressed considering a large variety of realistic scenarios, i.e. oil spills from ships, large accidental oil spills, natural oil seepages, etc. Each operational domain is characterized by different needs and purposes: the identification of polluters very often calls for the detection of small-size oil spills due to illicit operations from vessels; while the characterization of the chemical/physical properties of surfactants is desired in the case of remediation activities for minimizing pollution effects.

In this framework, the large polarimetric SAR data set nowadays available, characterized by different wavelength, resolution and coverage, offers an unprecedented opportunity to enhance sea oil slick observation. All the polarimetric approaches widely and successfully used allow exploiting the large amount of physical information to perform oil slick detection, discrimination and characterization overcoming the limitations presented by single-polarization techniques. Nevertheless, they need suitable electromagnetic models and analysis tools to be transformed in useful added-value products. All polarimetric approaches share a common physical rationale based on the departure from the slick-free sea surface Bragg scattering, which applies for intermediate incidence angles and under low-to-moderate regime, due to the presence of an oil slick. A large set of polarimetric features is critically reviewed in terms of oil detection, discrimination and characterization capabilities. A discussion on the role played by the SAR data quality (i.e. calibration, noise floor, etc.) within the frame of polarimetric features extraction is also addressed.

The performance of different SAR architectures is assessed with some thoughts experiments undertaken on actual L-band ALOS-PALSAR and C-band Radarsat-2 SAR data. The review clearly shows that all the polarimetric features allow detecting oil slicks and discriminating them from both weak-damping lookalikes and the surrounding sea. In some cases, this discrimination can be obtained without any external threshold. When possible, a fair ranking between different polarimetric features is performed according to a given set of polarimetric measurements. Therefore, all the considered SAR architectures offer the capability to provide at least rough information on the spatial variability of the damping properties of a given surfactant.

Hence, polarimetric methods can fully assist users in performing sea oil slick observation.

In reviewing sea oil slick observation literature, future trends mainly concern a deeper analysis of oil-in-water particles and oil in ice-infested scenarios. The latter are very challenging scenarios that call for proper models and analysis tools. In addition, the combination of more polarimetric features into multi-features seems to be a key point to enhance sea oil slick monitoring performance. From an operational oil service viewpoint, recently, the technological development that led to new SAR architectures as the staggered SAR and the CP architectures should be further investigated and exploited. To conclude, future works could involve a deeper analysis on the physical link between quad- and compact-polarimetric SAR architectures in order to exploit the high potential that the latter seem to have for operational sea oil slick observation.

Disclosure statement

No potential conflict of interest was reported by the authors.

References

Born, M., and E. Wolf. 1980. *Principles of Optics*. London: Cambridge University Press.

Brekke, C., B. Holt, C. Jones, and S. Skrunes. 2014. "Discrimination of Oil Spills from Newly Formed Sea Ice by Synthetic Aperture Radar." *Remote Sensing of Environment* 145: 1–14. doi:10.1016/j.rse.2014.01.015.

Brekke, C., and A. Solberg. 2005. "Oil Spill Detection by Satellite Remote Sensing." *Remote Sensing of Environment* 95 (1): 1–13. doi:10.1016/j.rse.2004.11.015.

Brekke, C., and A. Solberg. 2008. "Classifiers and Confidence Estimation for Oil Spill Detection in ENVISAT ASAR Images." *IEEE Geoscience and Remote Sensing Letters* 5 (1): 65–69. doi:10.1109/LGRS.2007.907174.

Cloude, S. R. 1986. "Group Theory and Polarisation Algebra." *Optik* 75 (1): 26–36.

Cloude, S. R. 2009. *Polarisation: Applications in Remote Sensing*. Oxford: Oxford University Press.

Cloude, S. R., D. G. Goodenough, and H. Chen. 2012. "Compact Decomposition Theory." *IEEE Geoscience and Remote Sensing Letters* 9 (1): 28–32. doi:10.1109/LGRS.2011.2158983.

Cloude, S. R., and E. Pottier. 1996. "A Review of Target Decomposition Theorems in Radar Polarimetry." *IEEE Transactions on Geoscience Remote Sensing* 34: 498–518. doi:10.1109/36.485127.

Cloude, S. R., and E. Pottier. 1997. "An Entropy Based Classification Scheme for Land Applications of Polarimetric SAR." *IEEE Transactions on Geoscience Remote Sensing* 35 (1): 68–78. doi:10.1109/36.551935.

Collins, M. J., M. Denbina, B. Minchew, C. E. Jones, and B. Holt. 2015. "On the Use of Simulated Airborne Compact Polarimetric SAR for Characterizing Oil–Water Mixing of the Deepwater Horizon Oil Spill." *IEEE Journal of Selected Topics in Applied Earth Observations and Remote Sensing* 8 (3): 1062–1077. doi:10.1109/JSTARS.2015.2401041.

Fingas, M. F., and C. E. Brown. 1997. "Review of Oil Spill Remote Sensing." *Spill Science & Technology Bulletin* 4: 199–208. doi:10.1016/S1353-2561(98)00023-1.

Fingas, M. F., and C. E. Brown. 2015. "Chapter 12: Oil Spill Remote Sensing." In *Handbook of Oil Spill Science and Technology*, edited by M. F. Fingas, 313–356. Hoboken, NJ: Wiley.

Gade, M., W. Alpers, H. Huhnerfuss, H. Masuko, and T. Kobayashi. 1998. "Imaging of Biogenic and Anthropogenic Ocean Surface Films by the Multifrequency/Multipolarization SIR-C/X-SAR." *Journal Geophysical Research* 103: 18851–18866.

Gade, M., H. Huhnerfuss, and G. Korenowski, eds. 2006. "Chapter 1: Basic Physiochemical Principles of Monomolecular Sea Slicks and Crude Oil Spills." In *Marine Surface Films*, 21–35. Berlin: Springer-Verlag.

Gambardella, A., G. Giacinto, M. Migliaccio, and A. Montali. 2010. "A One-Class Classification for Oil Spill Detection." *Pattern Analysis and Applications Journal* 13: 349–366. doi:10.1007/s10044-009-0164-z.

Gil, J. J. 2000. "Characteristic Properties of Mueller Matrices." *Journal of the Optical Society of America* 17: 328–334.

Gil, J. J. 2007. "Polarimetric Characterization of Light and Media." *The European Physical Journal Applied Physics* 40: 1–47. doi:10.1051/epjap:2007153.

Guissard, A. 1994. "Mueller and Kennaugh Matrices in Radar Polarimetry." *IEEE Transactions on Geoscience Remote Sensing* 32: 590–597. doi:10.1109/36.297977.

Jones, C. E., B. Minchew, B. Holt, and S. Hensley. 2011. "Studies of the Deepwater Horizon Oil Spill with the UAVSAR Radar." In *Monitoring and Modeling the Deepwater Horizon Oil Spill: A Record-Breaking Enterprise*, edited by Wiley, Geophysical Monograph Series, Vol. 9, 33–50. Washington, DC: AGU.

Kudryavtsev, V. N., B. Chapron, A. G. Myasoedov, F. Collard, and J. A. Johannessen. 2013. "On Dual Co-Polarized SAR Measurements of the Ocean Surface." *IEEE Geoscience and Remote Sensing Letters* 10 (4): 761–765. doi:10.1109/LGRS.2012.2222341.

Kumar, L. J. V., J. K. Kishore, and P. K. Rao. 2014. "Decomposition Methods for Detection of Oil Spills Based on RISAT-1 SAR." *International Journal of Remote Sensing & Geoscience* 3 (4): 21–27.

Lee, J. S., and E. Pottier. 2009. *Polarimetric Radar Imaging: From Basics to Applications*. Boca Raton, FL: CRC Press, Taylor & Francis Group.

Li, H., W. Perrie, Y. He, J. Wu, and X. Luo. 2015. "Analysis of the Polarimetric SAR Scattering Properties of Oil-Covered Waters." *Journal of Selected Topics on Applied Earth Observation* PP (99): 1–9.

Mandel, L., and E. Wolf. 1995. *Optical Coherence and Quantum Optics*. New York: Cambridge University Press.

Matkan, A. A., M. Hajeb, and Z. Azarakhsh. 2014. "Assessment of Capability of the Target Decomposition Features in Sea Oil Pollution Detection Using Polarimetric SAR Data." *Journal of Radar* 2 (3): 13–23.

Migliaccio, M., A. Gambardella, F. Nunziata, M. Shimada, and O. Isoguchi. 2009. "The PALSAR Polarimetric Mode for Sea Oil Slick Observation." *IEEE Transactions on Geoscience Remote Sensing* 47: 4032–4041. doi:10.1109/TGRS.2009.2028737.

Migliaccio, M., A. Gambardella, and M. Tranfaglia. 2007. "SAR Polarimetry to Observe Oil Spills." *IEEE Transactions on Geoscience Remote Sensing* 45: 506–511. doi:10.1109/TGRS.2006.888097.

Migliaccio, M., and F. Nunziata. 2014. "On the Exploitation of Polarimetric SAR Data to Map Damping Properties of the Deepwater Horizon Oil Spill." *International Journal of Remote Sensing* 35 (10): 3499–3519. doi:10.1080/01431161.2014.905730.

Migliaccio, M., F. Nunziata, C. E. Brown, B. Holt, X. Li, W. G. Pichel, and M. Shimada. 2012. "Polarimetric Synthetic Aperture Radar Utilized to Track Oil Spills." *Transaction on EOS, American Geophysical Union* 93 (16): 161–163.

Migliaccio, M., F. Nunziata, and A. Gambardella. 2009. "On the Co-Polarized Phase Difference for Oil Spill Observation." *International Journal of Remote Sensing* 30: 1587–1602. doi:10.1080/01431160802520741.

Migliaccio, M., F. Nunziata, A. Montuori, and C. E. Brown. 2012. "Marine Added-value Products Using RADARSAT-2 Fine Quad-polarization." *Canadian Journal of Remote Sensing* 37 (5): 443–451. doi:10.5589/m11-054.

Migliaccio, M., F. Nunziata, A. Montuori, X. Li, and W. Pichel. 2011. "A Multi-frequency Polarimetric SAR Processing Chain to Observe Oil Fields in the Gulf of Mexico." *IEEE*

Transactions on Geoscience Remote Sensing 49 (12): 4729–4737. doi:10.1109/TGRS.2011.2158828.

Minchew, B. 2012. "Determining the Mixing of Oil and Sea Water Using Polarimetric Synthetic Aperture Radar." *Geophysical Research Letters* 39 (16): 1–6. doi:10.1029/2012GL052304.

Minchew, B., C. E. Jones, and B. Holt. 2012. "Polarimetric Analysis of Backscatter from the Deepwater Horizon Oil Spill Using L-Band Synthetic Aperture Radar." *IEEE Transactions on Geoscience Remote Sensing* 50 (10): 3812–3830. doi:10.1109/TGRS.2012.2185804.

National Oceanic and Atmospheric Administration (NOAA). 2012. "Natural Resource Damage Assessment: Status Update for the Deepwater Horizon Oil Spill." http://www.gulfspillrestoration.noaa.gov

National Research Council (US) Committee on Oil in the Sea. 2003. *Oil in the Sea III: Inputs, Fates, and Effects*. Washington, DC: National Academies Press (US). http://www.ncbi.nlm.nih.gov/books/NBK220703/

Nghiem, S. V., S. H. Yueh, R. Kwok, and F. K. Li. 1992. "Symmetry Properties in Polarimetric Remote Sensing." *Radio Science* 27 (5): 693–711. doi:10.1029/92RS01230.

Nunziata, F., A. Gambardella, and M. Migliaccio. 2008. "On the Mueller Scattering Matrix for SAR Sea Oil Slick Observation." *IEEE Geoscience and Remote Sensing Letters* 5: 691–695. doi:10.1109/LGRS.2008.2003127.

Nunziata, F., A. Gambardella, and M. Migliaccio. 2012. "A Unitary Mueller-based View of Polarimetric SAR Oil Slick Observation." *International Journal of Remote Sensing* 33 (20): 6403–6425. doi:10.1080/01431161.2012.687474.

Nunziata, F., A. Gambardella, and M. Migliaccio. 2013. "On the Degree of Polarization for SAR Sea Oil Slick Observation." *ISPRS Journal of Photogrammetry and Remote Sensing* 78: 41–49. doi:10.1016/j.isprsjprs.2012.12.007.

Nunziata, F., and M. Migliaccio. 2014. "International Oil Spill Response Technical Seminar: Oil Spill Monitoring and Damage Assessment via PolSAR Measurements." In *Aquatic Procedia*, edited by X. Li, 1–8. Elsevier. www.sciencedirect.com

Nunziata, F., M. Migliaccio, and A. Gambardella. 2011. "Pedestal Height for Oil Spill Observation." *IET Radar Sonar and Navigation* 5: 103–110.

Nunziata, F., M. Migliaccio, and X. Li. 2015. "Sea Oil Slick Observation Using Hybrid-Polarity SAR Architecture." *Journal of Oceanic Engineering* 40 (2): 426–440.

Nunziata, F., P. Sobieski, and M. Migliaccio. 2009. "The Two-Scale BPM Scattering Model for Sea Biogenic Slicks Contrast." *IEEE Transactions on Geoscience Remote Sensing* 47 (7): 1949–1956. doi:10.1109/TGRS.2009.2013135.

Paes, R. L., F. Nunziata, and M. Migliaccio. Forthcoming. "On the Capability of Hybrid-Polarity Features to Observe Metallic Targets at Sea." *Journal of Oceanic Engineering*. doi:10.1109/JOE.2015.2424751.

Praks, J., E. C. Koeniguer, and M. T. Hallikainen. 2009. "Alternatives to Target Entropy and Alpha Angle in SAR Polarimetry." *IEEE Transactions on Geoscience Remote Sensing* 47: 2262–2274. doi:10.1109/TGRS.2009.2013459.

Raney, R. K. 2007. "Hybrid-Polarity SAR Architecture." *IEEE Transactions on Geoscience Remote Sensing* 45 (11): 3397–3404. doi:10.1109/TGRS.2007.895883.

Raney, R. K. 2011. "A Perspective on Compact-polarimetry." *IEEE Geoscience and Remote Sensing Newsletter* 160: 12–18.

Raney, R. K., J. T. S. Cahill, G. W. Patterson, and D. B. Bussey. 2012. "The M-Chi Decomposition of Hybrid Dual-Polarimetric Radar Data with Application to Lunar Craters." *Journal of Geophysical Research: Planets* 117 (E12): 1–8. doi:10.1029/2011JE003986.

Raney, R. K., P. D. Spudis, B. Bussey, J. Crusan, J. R. Jensen, W. Marinelli, P. McKerracher, C. Neish, M. Palsetia, R. Schulze, H. B. Sequeira, and H. Winters. 2011. "The Lunar Mini-RF Radars: Hybrid Polarimetric Architecture and Initial Results." *Proceedings of the IEEE* 99 (5): 808–823. doi:10.1109/JPROC.2010.2084970.

Sabry, R., and P. W. Vachon. 2014. "A Unified Framework for General Compact and Quad Polarimetric SAR Data and Imagery Analysis." *IEEE Transactions on Geoscience Remote Sensing* 52 (1): 582–602. doi:10.1109/TGRS.2013.2242479.

Salberg, A.-B., O. Rudjord, and A. H. S. Solberg. 2014. "Oil Spill Detection in Hybrid-Polarimetric SAR Images." *IEEE Transactions on Geoscience Remote Sensing* 52 (10): 6521–6533. doi:10.1109/TGRS.2013.2297193.

Sarabandi, K. 1992. "Derivation of Phase Statistics from the Mueller Matrix." *Radio Science* 27: 553–560. doi:10.1029/92RS00195.

Shirvany, R., M. Chabert, and J. Tourneret. 2012. "Ship and Oil Spill Detection Using the Degree of Polarization in Linear and Hybrid/Compact Dual-pol SAR." *Journal of Selected Topics on Applied Earth Observation* 5 (3): 885–892. doi:10.1109/JSTARS.2012.2182760.

Skrunes, S., C. Brekke, and A. P. Doulgeris. 2015. "Characterization of Low-Backscatter Ocean Features in Dual-Copolarization SAR Using Log-Cumulants." *IEEE Geoscience and Remote Sensing Letters* 12 (4): 836–840. doi:10.1109/LGRS.2014.2363688.

Skrunes, S., C. Brekke, and T. Eltoft. 2014. "Characterization of Marine Surface Slicks by Radarsat-2 Multipolarization Features." *IEEE Transactions on Geoscience Remote Sensing* 52 (9): 5302–5319. doi:10.1109/TGRS.2013.2287916.

Skrunes, S., C. Brekke, T. Eltoft, and V. Kudryavtsev. 2014. "Comparing Near-Coincident C- and X-B and SAR Acquisitions of Marine Oil Spills." *IEEE Transactions on Geoscience Remote Sensing* 55 (4): 1958–1975.

Solberg, A., C. Brekke, and P. Husoy. 2007. "Oil Spill Detection in Radarsat and Envisat SAR Images." *IEEE Transactions on Geoscience Remote Sensing* 45 (3): 746–755. doi:10.1109/TGRS.2006.887019.

Solberg, A. H. S. 2012. "Remote Sensing of Ocean Oil Spill Pollution." *Proceedings of the IEEE* 100 (10): 2931–2945. doi:10.1109/JPROC.2012.2196250.

Solberg, A. H. S., G. Storvik, R. Solberg, and E. Volden. 1999. "Automatic Detection of Oil Spills in ERS SAR Images." *IEEE Transactions on Geoscience Remote Sensing* 37 (4): 1916–1924. doi:10.1109/36.774704.

Touzi, R., C. E. Livingstone, J. R. C. Lafontaine, and T. I. Lukowski. 1993. "Consideration of Antenna Gain and Phase Patterns for Calibration of Polarimetric SAR Data." *IEEE Transactions on Geoscience Remote Sensing* 31 (6): 1132–1145. doi:10.1109/36.317449.

Touzi, R., P. W. Vachon, and J. Wolfe. 2010. "Requirement on Antenna Cross-Polarization Isolation for the Operational Use of C-Band SAR Constellations in Maritime Surveillance." *IEEE Geoscience and Remote Sensing Letters* 7 (4): 861–865. doi:10.1109/LGRS.2010.2053835.

Valentine, D. L., G. B. Fisher, S. C. Bagby, R. K. Nelson, C. M. Reddy, S. P. Sylva, and M. A. Woo. 2014. "Fallout Plume of Submerged Oil from Deepwater Horizon." *Proceedings of the National Academy of Sciences of the United States of America* 111 (45): 15906–15911. doi:10.1073/pnas.1414873111.

Van Zyl, J. J., C. H. Papas, and C. Elachi. 1987. "On the Optimum Polarizations of Incoherently Reflected Waves." *IEEE Transactions on Antennas and Propagation* 35: 818–825. doi:10.1109/TAP.1987.1144175.

Velotto, D., M. Migliaccio, F. Nunziata, and S. Lehner. 2011. "Dual-polarized TerraSAR-X Data for Oil Spill Observation." *IEEE Transactions on Geoscience Remote Sensing* 30: 1587–1602.

Villano, M., G. Krieger, and A. Moreira. 2014. "Staggered SAR: High-Resolution Wide-Swath Imaging by Continuous PRI Variation." *IEEE Transactions on Geoscience Remote Sensing* 52 (7): 4462–4479. doi:10.1109/TGRS.2013.2282192.

Woods Hole Oceanographic Institution (WHOI). 2011. "Oil in the Ocean: Natural Oil Seeps." Athens, Greece. http://www.whoi.edu/oil/natural-oil-seeps

Yin, J. J., J. Yang, Z.-S. Zhou, and J. Song. Forthcoming. "The Extended Bragg Scattering Model-Based Method for Ship and Oil-Spill Observation Using Compact Polarimetric SAR." *IEEE Journal Selected Topics Applied Earth Observation Remote Sensing*, 1–13. doi:10.1109/JSTARS.2014.2359141.

Zhang, B., W. Perrie, X. Li, and W. G. Pichel. 2011. "Mapping Sea Surface Oil Slicks Using Radarsat-2 Quad-polarization SAR Image." *Geophysical Research Letters* 38 (10): 1–5. doi:10.1029/2011GL047013.